LITERATURE CITED

Ankel-Simons F. 2000. Primate anatomy, 2nd ed. San Diego: Academic Press.

Conroy GC, Mahoney CJ. 1991. Mixed longitudinal study of dental emergency in the chimpanzee. *Pan troglodytes* (Primates, Pongidae). Am J Phys Anthropol 86:243–254.

Crelin ES. 1987. The human vocal tract. New York: Vantage Press.

Crompton AW, German RZ, Thexton AJ. 1997. Mechanism of swallowing and airway protection in infant mammals (*Sus domesticus* and *Macaca fascicularis*). J Zool 241:89–102.

Ekberg O. 1982. Closure of the laryngeal vestibule during deglutition. Acta Otolaryngol 93:123–129.

Ekberg O, Sigurjónsson SV. 1982. Movement of the epiglottis during deglutition. A cineradiographic study. Gastrointest Radiol 7:101–107.

Fant G. 1960. Acoustic theory of speech production. The Hague: Mouton.

Fitch WT. 2000a. The evolution of speech: a comparative review. Trends Cogn Sci 4:258–267.

Fitch WT. 2000b. The phonetic potential of nonhuman vocal tracts: comparative cineradiographic observations of vocalizing animals. Phonetica 57:205–218.

Fitch WT, Giedd J. 1999. Morphology and development of the human vocal tract: a study using magnetic resonance imaging. J Acoust Soc Am 106:1511–1522.

Fitch WT, Reby D. 2001. The descended larynx is not uniquely human. Proc Biol Sci 268:1669–1675.

Flügel C, Rohen JW. 1991. The craniofacial proportions and laryngeal position in monkeys and man of different ages. (A morphometric study based on CT-scans and radiographs). Mech Aging Dev 61:65–83.

Hayama S. 1970. The *Saccus laryngis* in primates. J Anthropol Soc Nippon 78:274-298 (in Japanese with English abstract).

Hewitt G, MacLarnon A, Jones KE. 2002. The functions of laryngeal air sac in primates: a new hypothesis. Folia Primatol 73:70–94.

Hiiemae KM. 2000. The oro-facial complex in macaques: tongue and jaw movements in feeding. In: Whitehead PF, Jolly CJ, editors. Old world monkeym. Cambridge: Cambridge University Press.

Hiiemae KM, Hayenga SM, Reese A. 1995. Patterns of tongue and jaw movement in a cineradiographic study of feeding in the macaque. Arch Oral Biol 3:229–246.

Hiiemae KM, Palmer JB. 1999. Food transport and bolus formation during complete feeding sequences on foods of different initial consistency. Dysphagis 14:31–42.

Hiiemae KM, Palmer JB. 2003. Tongue movements in feeding and speech. Crit Rev Oral Biol Med 14:413–429.

Hiiemae KM, Palmer JB, Medicis SW, Hegener J, Jackson BS, Lieberman DE. 2002. Hyoid and tongue surface movements in specking and eating. Arch Oral Biol 47:11–27.

Hurme VO. 1949. Ranges of normalcy in the eruption of permanent teeth. J Dent Child 16:11–15.

Iwamoto M, Hamada Y, Watanabe T. 1984. Eruption of deciduous teeth in Japanese macaques (*Macaca fuscata*). J Anthropol Soc Nippon 92:273-279 (in Japanese with English abstract).

Iwamoto M, Watanabe T, and Hamada Y. 1987. Eruption of permanent teeth in Japanese monkeys (*Macaca fuscata*). Primate Res 3:18-28 (in Japanese with English abstract).

Kuykendall KL, Mahoney CJ, Conroy GC. 1992. Probit and survival analysis of tooth emergency ages in a mixed-longitudinal sample of chimpanzees (*Pan troglodytes*). Am J Phys Anthropol 89:379–399.

Laitman JT, Crelin ES, Conlogue GJ. 1977. The function of the epiglottis in monkey and man. Yale J Biol Med 50:43–48.

Laitman JT, Reidenberg JS. 1993. Specialization of the human upper respiratory and upper digestive system as seen through comparative and developmental anatomy. Dysphasia 8:318–325.

Larson JE, Herring SW. 1996. Movement of the epiglottis in mammals. Am J Phys Anthropol 100:71–82.

Lieberman DE, McCarthy RC. 1999. The ontogeny of cranial base angulation in humans and chimpanzees and its implications for reconstructing pharyngeal dimensions. J Hum Evol 36:487–517.

Lieberman DE, McCarthy RC, Hiiemae KM, Palmer JB. 2001. Ontogeny of postnatal hyoid and larynx descent in humans. Arch Oral Biol 46:117–128.

Lieberman P. 1984. The biology and evolution of language. Cambridge, MA: Harvard University Press.

Lieberman P, Blumstein SE. 1988. Speech physiology, speech perception, and acoustic phonetics. Cambridge, MA: Harvard University Press.

Lieberman PH, Klatt DH, Wilson WH. 1969. Vocal tract limitations on the vowel repertoires of rhesus monkey and other nonhuman primates. Science 164:1185–1187.

Lysell L, Magnusson B, Thilander B. 1962. Time and order of eruption of the primary teeth: a longitudinal study. Odont Revy 13:217–234.

Negus V. 1949. The comparative anatomy and physiology of the larynx. London: William Heinemann Medical Books.

Nishimura T. 2003. Comparative morphology of the hyo-laryngeal complex in anthropoids: two steps in the evolution of the descent of the larynx. Primates 44:41–49.

Nishimura T. 2005. Developmental changes in the shape of the supralaryngeal vocal tract in chimpanzees. Am J Phys Anthropol 126:193–204.

Nishimura T. 2006. Descent of the larynx in chimpanzees: mosaic and multiple-step evolution of the foundations for human speech. In: Matsuzawa T, Tomonaga M, Tanaka M, editors. Cognitive development in chimpanzees. Tokyo: Springer-Verlag. p 75-95.

Nishimura T, Mikami A, Suzuki J, Matsuzawa T. 2003. Descent of the larynx in chimpanzee infants. Proc Nat Acad Sci USA 100:6930–6933.

Nishimura T, Mikami A, Suzuki J, Matsuzawa T. 2006. Descent of the hyoid in chimpanzees: evolution of face flattening and speech. J Hum Evol 51:244–254.

Nishimura T, Mikami A, Suzuki J, Matsuzawa T. 2007. Development of the laryngeal air sac in chimpanzees. Int J Primatol 28:483–492.

Primate Research Institute, Kyoto University. 2002. Guide for the care and use of laboratory primates, 2nd ed. Inuyama: Primate Research Institute, Kyoto University.

Reidenbach MM. 1997. Anatomical considerations of closure of the laryngeal vestibule during swallowing. Eur Arch Otorhinolaryngol 254:410–412.

Riede T, Bronson E, Hatzikirou H, Zuberbühler K. 2005. Vocal production mechanisms in a non-human primate: morphological data and a model. J Hum Evol 48:85–96.

Roche AF, Barkla DH. 1965. The level of the larynx during childhood. Ann Otol Rhinol Laryngol 74:645–654.

Sasaki CT, Levine PA, Laitman JT, Crelin ES. 1977. Postnatal descent of the epiglottis in man: a preliminary report. Arch Otolaryngol 103:169–171.

Smith BH. 1991. Standard of human tooth formation and dental age assessment. In: Kelley MA, Larsen CS, editors. Advances in dental anthropology. New York: Wiley-Liss. p 143-168.

Smith BH, Garn SM. 1987. Polymorphisms in eruption sequence of permanent teeth in American children. Am J Phys Anthropol 74:289–303.

Starck D, Schneider R. 1960. Respirationsorgane: A. Larynx. In: Hofer H, Schultz AH, Starck D, editors. Primatologia, Vol. 3-2. Basel: Karger. p 423–587.

Stevens KN. 1998. Acoustic phonetics. Cambridge, MA: MIT Press.

Swindler DR, Wood CD. 1973. An atlas of primate gross anatomy. Baboon, chimpanzees, and man. Seattle: University of Washington Press.

Takemoto H. 2001. Morphological analyses of the human tongue musculature for three-dimensional modeling. J Speech Lang Hearing Res 44:95–107.

Titze IR. 1994. Principles of voice production. Englewood Cliffs: Prentice-Hall.

Vandaele DJ, Perlman AL, Cassell MD. 1995. Intrinsic fibre architecture and attachments of the human epiglottis and their contributions to the mechanism of deglutition. J Anat 186:1–15.

Vorperian HK, Kent RD, Gentry LR, Yandell BS. 1999. Magnetic resonance imaging procedures to study the concurrent anatomic development of vocal tract structures: preliminary results. Int J Pediat Otorhinolaryngol 49:197–206.

Williams PL, editor. 1995. Gray's anatomy, 38th ed. New York: Churchill Lavingstone.

Westhorpe RN. 1987. The position of the larynx in children and its relationship to ease of intubation. Anaesth Intens Care 15: 384–388.

Zemlin WR. 1988. Speech and hearing science: anatomy and physiology, 3rd ed. Englewood Cliffs: Prentice-Hall.

Available online at www.sciencedirect.com

ScienceDirect

Journal of Nutritional Biochemistry 19 (2008) 524–535

Journal of Nutritional Biochemistry

Allicin inhibits cell growth and induces apoptosis through the mitochondrial pathway in HL60 and U937 cells

Talia Miron[a,*], Meir Wilchek[a], Ayala Sharp[b], Yoshihito Nakagawa[c], Makoto Naoi[c], Yoshinori Nozawa[c], Yukihiro Akao[c]

[a]*Department of Biological Chemistry, Weizmann Institute of Science, Rehovot 76100, Israel*
[b]*Department of Biological Services, Weizmann Institute of Science, Rehovot 76100, Israel*
[c]*Gifu International Institute of Biotechnology, Kakamigahara, Gifu 504-0838, Japan*

Received 22 April 2007; received in revised form 12 June 2007; accepted 20 June 2007

Abstract

In this article, the effects of allicin, a biological active compound of garlic, on HL60 and U937 cell lines were examined. Allicin induced growth inhibition and elicited apoptotic events such as blebbing, mitochondrial membrane depolarization, cytochrome *c* release into the cytosol, activation of caspase 9 and caspase 3 and DNA fragmentation. Pretreatment of HL60 cells with cyclosporine A, an inhibitor of the mitochondrial permeability transition pore (mPTP), inhibited allicin-treated cell death. HL60 cell survival after 1 h pretreatment with cyclosporine A, followed by 16 h in presence of allicin (5 μM) was ~80% compared to allicin treatment alone (~50%). Also *N*-acetyl cysteine, a reduced glutathione (GSH) precursor, prevented cell death. The effects of cyclosporine A and *N*-acetyl cysteine suggest the involvement of mPTP and intracellular GSH level in the cytotoxicity. Indeed, allicin depleted GSH in the cytosol and mitochondria, and buthionine sulfoximine, a specific inhibitor of GSH synthesis, significantly augmented allicin-induced apoptosis. In HL60 cells treated with allicin (5 μM, 30 min) the redox state for 2GSH/oxidized glutathione shifted from E_{GSH} −240 to −170 mV. The same shift was observed in U937 cells treated with allicin at a higher concentration for a longer period of incubation (20 μM, 2 h). The apoptotic events induced by various concentrations of allicin correlate to intracellular GSH levels in the two cell types tested (HL60: 3.7 nmol/10^6 cells; U937: 7.7 nmol/10^6 cells). The emerging mechanistic basis for the antiproliferative function of allicin, therefore, involves the activation of the mitochondrial apoptotic pathway by GSH depletion and by changes in the intracellular redox status.

Keywords: Allicin; Apoptosis; Garlic; GSH; HL60; U937

1. Introduction

Allicin, diallyl thiosulfinate, is the main biologically active compound derived from garlic. It is produced by the interaction of the enzyme alliinase (alliin lyase; EC 4.4.1.4) with its substrate alliin (*S*-allyl-L-cysteine sulfoxide) [1]. Since alliinase and alliin are enclosed in different compartments within the garlic clove cells, intact garlic cloves do not contain allicin. When the garlic clove is crushed, alliin and alliinase interact, to form allicin, pyruvic acid and ammonia (Scheme 1). Allicin became an object of interest due to its potential to confer a vast spectrum of health beneficial effects including: anti microbial, antifungal and antiparasitic [2], antihypertensive [3], cardioprotective [4–6], anti-inflammatory [7] and anticancer activities [2,8,9].

In vitro studies of allicin's effect on human mammary MCF-7 cancer cells revealed that its antiproliferative activity is accompanied by accumulation of cells in the regulatory checkpoints, G_0/G_1 and G_2/M, of the cell cycle [9]. Interestingly, also other ally sulfur compound cause similar effects [10]. Allicin was shown to induce apoptosis in gastric

Abbreviations: BSO, D,L-buthionine *S,R*-sulfoximine; CsA, Cyclosporin A; DTNB, 5,5′-dithiobis-(2-nitrobenzoic acid); GGCS, γ-Glutamyl-L-cysteine synthetase; GSH, Reduced glutathione; GSSA, *S*-allylmercaptoglutathione; GSSG, Oxidized glutathione; mPTP, Mitochondrial permeability transition pore; NAC, *N*-acetyl-L-cysteine; XTT, 2,3-Bis (2-methoxy-4-nitro-5-sulfophenyl)-2*H*-tetrazolium-5-carboxanilide sodium salt.

* Corresponding author. Tel.: +972 8 9343627; fax: +972 8 9468256.
E-mail address: talia.miron@weizmann.ac.il (T. Miron).

0955-2863/$ – see front matter © 2008 Elsevier Inc. All rights reserved.
doi:10.1016/j.jnutbio.2007.06.009

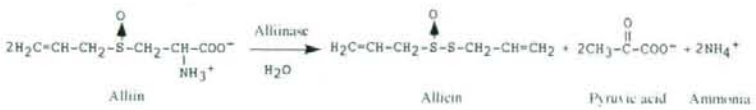

Scheme 1.

cancer SGC-7901 cells. The cause of apoptosis was related to decreased telomerase activity, an enzyme which allicin inhibits in a time- and dose- dependent manner [11]. Allicin induces apoptosis in human cervical cancer SiHa cells and mouse fibroblast-like L-929 cells, manifested through the appearance of characteristic apoptotic morphological changes in apoptotic bodies, through DNA fragmentation, and activation of caspases 8, 9 and 3 [12]. Allicin was also shown to induce apoptosis in human epithelial carcinoma through a caspase-independent pathway, mediated by the release of apoptotic-inducing factor (AIF) from mitochondria and protein kinase A (PKA) activation [13]. More results describing the effects of allicin or other garlic-derived products on various proteins participate in the apoptotic process have already been reported [14]. However, the mechanism underlying the induction of cell death by allicin has not been fully elucidated.

Apoptosis is an ordered cascade of events that culminates in cell death. Two main pathways of apoptosis have been characterized. The extrinsic pathway is initiated through ligand stimulation of the cell surface death receptors such as TNFR or CD95R. In this pathway, cell death is executed via a cascade of proteolytic events with the sequential activation of caspase 8 and caspase 3. The intrinsic pathway is triggered by mitochondrial stress caused by various factors such as DNA damage, oxidative stress and heat shock (reviewed [15]). This pathway is initiated through the release of signal factors from mitochondria as a consequence of mitochondrial membrane permeability transition. Such changes lead to translocation of pro- and antiapoptotic proteins across the mitochondrial membranes [16,17]. Among these proteins is cytochrome *c*, which is released from the mitochondria to the cytosol and participates with other molecules in the formation of a complex that activates caspase 9, which in turn activates caspase 3. The activation of these caspases leads to the final fragmentation of nuclear DNA, with the typical apoptotic morphological manifestations.

Allicin easily diffuses through cell membranes (diffusion coefficient 5×10^{-8} cm^2s^{-1}) [18] and exerts its biological effects by reacting with free thiols within the cell. In living cells, reduced glutathione (GSH) is the major free thiol participating in cellular redox reactions and mixed disulfide formation. GSH is therefore the main cellular target of allicin reaction (Scheme 2). Both allicin and its glutathione derivative, *S*-allylmercaptoglutathione (GSSA), can prevent the formation of free radicals. GSSA is similar in this preventive capacity to GSH, both being less effective in this antioxidant activity than allicin [19–21]. Allicin can scavenge the chain-carrying peroxyl radicals of the substrates by transferring its allylic hydrogen to the oxidized substrate. This renders it a stronger antioxidant than its derivatives [22].

Allicin is a short-lived compound, which rapidly reacts with free intracellular thiol groups [18,19,22]. It was found to disintegrate in the blood a few minutes after its administration, both in vitro in human blood [23] and in vivo in rats [24]. Therefore, the therapeutic effect of allicin administered orally may be restricted to targets that are close to the gastrointestinal tract. However, its main oxidation products, *S*-allylmercapto-glutathione and *S*-allylmercapto-cysteine, could exert their action in more remote sites within the body because they are more stable. The rapid disappearance of allicin can be exploited in tumor cells targeting. We previously showed that allicin kills tumor cells in vitro [25,26] and also in vivo if generated on their surface by conjugating alliinase to monoclonal antibodies directed to specific cell-surface receptors, such as ErbB2, overexpressed in breast and ovarian cancer [25]; CD20, a receptor expressed at high levels in human B chronic lymphocytic leukemia and other B-cell lymphomas [26].

The redox environment of a cell reflects the sum of the products of the reduction potential and the reducing capacity of the linked redox couples operating within the cell [27,28] Glutathione is considered to be the major thiol-disulfide redox buffer of cells [29]. The redox state of the 2GSH/oxidized glutathione (GSSG) redox couple depends on their molar ratio. Upon reacting with GSH, allicin causes a decrease in free GSH concentration and an increase in mixed-disulfide glutathione products, which leads to an increase in the reduction potential values. Allicin also reacts with other

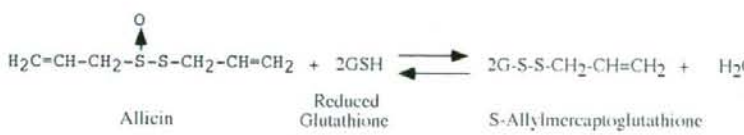

Scheme 2.

free sulfhydril (SH)-bearing molecules in the cell, such as cysteine and SH residues in proteins, yet their relatively low concentrations contribute only little towards changing the reduction potential of the cell upon oxidation. The reduction potential of cells was proposed to reflect their growth cycle. Accordingly, the reduction potential of proliferating cells (pH 7.0) is E_{GSH} −240 mV. Increased values (E_{GSH} −200 mV) represent differentiation, and a further oxidative shift to a higher value (E_{GSH} −170 mV) elicits apoptosis [27]. In this study, we aimed to examine the initial events leading to apoptosis upon allicin treatment and the dependence of the apoptotic pathway on the reduction potential of cells.

2. Materials and methods

Alliin was synthesized from L-cysteine and allyl bromide followed by H_2O_2 oxidation [30]. Allicin (purity ~98%) was produced by applying synthetic alliin onto an immobilized alliinase column and its concentration was determined by high-performance liquid chromatography, as previously described [31].

2,3-Bis (2-methoxy-4-nitro-5-sulfophenyl)-2 *H*-tetrazolium-5-carboxanilide (XTT) sodium salt; D,L-buthionine *S*, *R*-sulfoximine (BSO); cyclosporin A (CsA); *N*-acetyl-L-cysteine (NAC); 5,5′-dithiobis-(2-nitrobenzoic acid) (DTNB); metaphosphoric acid; phenazine methosulfate (PMS) and 2-vinylpyridine were purchased from Sigma Chemical (St. Louis, MO, USA).

2.1. Cell culture, cell viability and morphological studies.

HL60 human promyelocytic leukemia-derived cells and U937 human myelomonocytic cells were maintained in RPMI-1640 supplemented with 2 mM L-glutamine, 10% (v/v) fetal bovine serum and antibiotics. Cell viability was measured using the XTT assay, based on the reduction of tetrazolium salt to soluble formazan compounds by mitochondrial enzymes. Cells (15.000–20.000 cells/well) were seeded in a 96-well plate. After 16-h incubation with allicin, in the presence or absence of NAC (0.1–1.0 mM) or after 16 h incubation with BSO (0.1 mM) alone, 50 μl of XTT/PMS mixture (50 μM PMS, 0.1% XTT in medium) were added onto the cells. After an incubation period of 3–4 h at 37°C, the absorbance of the samples was measured in an enzyme-linked immunosorbent assay (ELISA) reader at 450 nm. SDS (1%, 10 μl/well) was added to reference wells before adding the XTT/PMS solution.

HL60 cells (300,000/ml) were pretreated with CsA for 1 h. Cells were seeded in a 96-well plate (20,000 cells/well) in the presence of allicin. The viability was tested by the XTT assay. The analysis of apoptotic morphological changes was done by staining cells with Hoechst 33342 at 37°C for 30 min in medium, washing with phosphate-buffered saline (PBS) and examining by fluorescence microscopy. For evaluating DNA ladder formation, cellular DNA was extracted from cells by ethanol precipitation of the phenol/chloroform extract [32]. After electrophoresis (5–10 μg DNA/lane) on an agarose (2.5%) gel, DNA was visualized by ethidium bromide staining.

Mitochondrial membrane potential was measured by using the fluorescent dye, Mito Tracker Red CMXRos (Molecular Probes, Eugene, OR, USA) that accumulates selectively in active mitochondria. Cells were washed with medium, incubated with Mito-Tracker Red CMXRos for 30 min at 37°C, washed with PBS and examined under fluorescence microscopy (Olympus, Tokyo).

Mitochondria were prepared from cultured cells (5–10×10^7) as described elsewhere [33]. Cells were harvested and washed with PBS (600 g, 7 min). Cell pellets were suspended in 0.5 ml cold hepes isotonic mitochondrial buffer (HIM) buffer (200 mM mannitol, 70 mM sucrose, 1 mM EGTA, 10 mM HEPES-KOH buffer, pH 7.5) containing protease inhibitors, incubated 30 min on ice and homogenized by multiple passages through a 25-gauge needle (5/8 in.). Nuclei and unbroken cells were removed (1300 g, 8 min at 4°C). Protein and free SH were determined in the cytosol, supernatant (10,000 g, 30 min at 4°C) and in the mitochondria-enriched fraction (pellet, dissolved in HIM buffer containing 1% Triton X-100). Protein assay was done with the Biuret Reagent [34] or the BCA protein assay kit (Pierce, Rockford, IL, USA).

2.2. Cell cycle analysis

HL60 cells were pretreated with CsA (5 μM, 1 h) and then cultured further for 20 h in the presence or absence of allicin. After harvesting, washing and resuspending in 0.25 ml PBS, an equal volume of 0.005% propidium iodide solution containing 0.01% heated-RNase A and 0.3% Triton X-100 was added. Cells were analyzed by flow cytometry using fluorescence-activated cell sorting (Becton Dickinson FACScan Instrument using CellQuest software (BD Bioscience, San Jose, CA, USA).

2.3. Electrophoresis and Western blot analysis

Cell pellet was resuspended in lysis buffers A or B [32]. Lysis buffer A (2×PBS, 0.1% sodium dodecyl sulfate (SDS), 1% Nonidet P-40, 0.5% sodium deoxycholate) containing protease inhibitors was used to analyze of caspases 3, 8 and 9. Lysis buffer B (250 mM sucrose, 20 mM HEPES-KOH buffer, pH 7.5, 10 mM KCl, 1.5 mM $MgCl_2$, 1 mM EDTA, 1 mM EGTA, 1 mM dithiothreitol [DTT]) containing protease inhibitors was used to analyze the presence of cytochrome *c* in the cytosol as described above (Section 2.2), After centrifugation (10,000g, 30 min, 4°C) the supernatant was separated by SDS-polyacrylamide gel electrophoresis using 15% gel and transferred electrophoretically onto a polyvinylidene difluoride (PVDF) membrane (Du Pont, Boston, MA, USA). The membrane was incubated overnight at 4°C with the following antihuman antibodies: anti β-actin (Sigma–Aldrich), anti-caspase 3 (Santa Cruz Biotechnology, Santa Cruz, CA, USA), anti-caspase 8 (MBL, Nagoya, Japan), anti

caspase-9 (Novus Biological, Littleton, CO, USA) and anti cytochrome *c* (Upstate Biotechnology, Lake Placid, NY, USA). The membranes were washed with tris-buffered saline Tween-20 (TBST), incubated with HRP-conjugated secondary antibody for 1 h at room temperature and washed with TBST. Proteins were detected with an enhanced chemiluminescence (ECL) detection kit (New England Biolabs) and a chemiluminescence detector (LAS-1000, Fuji, Japan).

2.4. Determination of cell volume

The volume of nontreated cells was determined by calculating sphere volumes based on diameter measurement of 100 cells. Since the morphology of treated cells was not spherical, cell volume was estimated by weighing the pellet of $2–4\times10^6$ cells and evaluating the volume on the assumption of 1/1 w/v.

2.5. Assay for glutathione and free SH

Cells were collected (600 g, 7 min, 4°C), washed with PBS and the pellets were stored at −80°C. After protein precipitation with 5% metaphosphoric acid (0.2–0.3 ml/3×10^6 cells) by centrifugation (10,000g, for 30 min), the supernatant was used for GSH quantitation, and the pellet, dissolved in 0.2–0.3 ml of 0.5 M NaOH, was used for protein determination. To determine GSH in the supernatant, a glutathione assay kit (Calbiochem) was used. GSH and GSSG content were also determined by the glutathione reductase recycling assay before and after modification with 2-vinyl pyridine [35]. Samples (40 μl) were neutralized with 2 M triethanolamine (10 μl) in a 96-well plate. The reaction was started by adding 200 μl per well of 0.4 U/ml enzyme in 143 mM phosphate buffer pH 7.5 containing 0.3 mM reduced nicotinamide adenine dinucleotide phosphate, 0.6 mM DTNB and 6.25 mM EDTA. The initial rate of 5-thio-2-nitrobenzoic acid formation was monitored. Determination of GSSG was done 1 h after modification of the free SH with 9 M 2-vinyl pyridine (1 μl/well) at room temperature. Oxidized glutathione (0–6 nmol/well) served as a reference.

Total free SH content in cell extracts or in cytosolic and mitochondrial fractions (50 μl) was determined with DTNB in a 96-well plate. Samples were acidified with 5% metaphosphoric acid (50 μl/well) to stabilize the reduced state and neutralized with 2 M triethanolamine (50 μl/well). DTNB (50 μl of 1 mM solution in 50 mM phosphate buffer pH 7.2 containing 2 mM EDTA) was added. After 10 min of incubation, the absorbance was measured at 412 nm using an ELISA reader. GSH (0–20 nmol/well) precalibrated with DTNB served as a reference, using E_M 14150 M^{-1} at 412 nm [36]. Reduction potential was calculated by using the Nernst equation for GSSG/2GSH: $E_{GSH}=E_0-30\times\log([GSH]^2/[GSSG])$ [27].

2.6. Statistical analysis

Each experiment was performed at least three times, and the results were expressed as mean values± S.D. (n=2–6). The Student t test was used to determine the significance of differences between the mean values obtained for the two cell lines. Otherwise, the various treatments, were analyzed using one-way analysis of variance (ANOVA) followed by either Dunnett or Bonferroni's multiple comparison test, considering $P<05$ as significant.

3. Results

3.1. Allicin inhibited proliferation of HL60 and U937 cells

The proliferation rate of exponentially growing HL60 and U937 cells in the presence of allicin was determined at a density of 100,000 cells ml^{-1}. Cells were incubated with increasing concentrations of allicin (HL60: 0–10 μM; U937: 0–30 μM) for growing time periods up to 72 h. Cell viability was determined by the trypan blue dye exclusion assay. Allicin inhibited cell growth in a concentration-dependent manner (Figs. 1A and 2A for HL60 and U937, respectively). In the presence of 5 μM allicin, HL60 cells exhibited about 50% inhibition of proliferation after 22 h, and at 10 μM allicin after 22 h, the rate of inhibition reached 80% (Fig. 1A). HL60 cells were more sensitive to allicin than U937 cells. Inhibition of U937 cell proliferation reached 50% and 60% at 15 and 20 μM allicin, respectively, after 22 h (Fig. 2A). We therefore chose to continue the study of HL60 and U937 cells (100,000 cells/ml) at 5 and 20 μM allicin, respectively.

3.2. Allicin induced apoptosis in the cells

3.2.1. Morphological changes

Morphological changes indicating apoptotic processes were observed by staining the cells with Hoechst 33342. Distinct nuclear condensation was observed in HL60 cells treated with allicin (5 μM) for 16 h (Fig. 1B) and U937 cells treated with allicin (20 μM) for 40 h (Fig. 2B). In both allicin-treated cell lines, more than 90% of the cells showed blebbing after 2 h (Fig. 3A, lower panel).

3.2.2. DNA fragmentation

A DNA ladder appeared in allicin (5 μM)-treated HL60 cells 6 h after treatment, whereas in allicin (20 μM)-treated U937 cells, it appeared only after 40 h (Figs. 1C and 2C).

3.2.3. Cytochrome c release into cytoplasm and activation of caspases

To better understand the mechanism of allicin-induced apoptosis, Western blot analysis was used to detect apoptosis-related proteins. Increased amounts of cytochrome *c* appeared in the cytosol of allicin (5 μM)-treated HL60 cells after 2.5 h of incubation. An increase in cleaved caspase 9 appeared 4 and 6 h after adding allicin, and it gradually decreased to the basal level after 30 h. Cleaved caspase 3 appeared after 16 h and was still observed 30 h after the treatment (Fig. 3B). U937 cells reacted at a slower rate to allicin (20 μM) treatment. Cytochrome *c* release into the cytosol began 6 h after adding allicin and reached a maximal

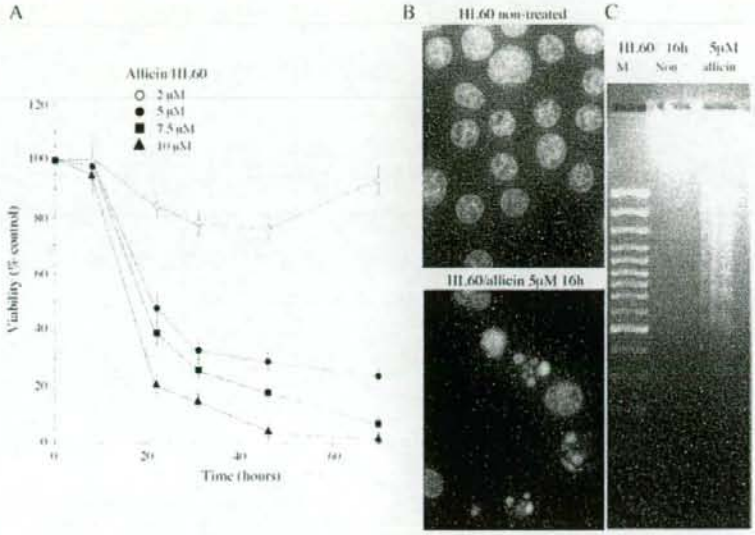

Fig. 1. Effect of allicin on cell growth of human leukemia HL60 cells. (A) Growth dependent of HL60 cells on allicin concentration. Viable cells were counted at various time intervals between 0–72 h after staining with trypan blue. Data represent the mean value of % viable cells (nontreated=100%)±S.D. (B) Apoptotic changes observed after Hoechst 33342 (5 μg/ml) staining for 30 min. Cells were treated with 5 μM allicin for 16 h. (C) Nucleosomal DNA fragmentation of nontreated cells and allicin-treated HL60 cells (5 μM, 6 h, 5 μg/lane). Lane M is a DNA size marker.

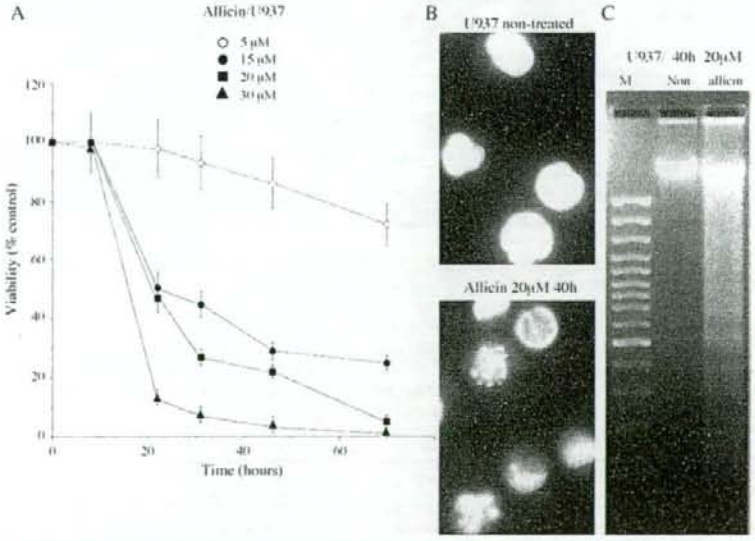

Fig. 2. Effect of allicin on cell growth of human leukemia U937 cells. (A) Growth dependence of U937 cells on allicin concentration. Viable cells were counted at various time intervals between 0–72 h after staining with trypan blue. Data represent the mean value of % viable cells (nontreated=100%)±S.D. (B) Hoechst 33342 (5 μg/ml) staining for 30 min of cells treated with 20 μM allicin for 40 h. (C) Nucleosomal DNA fragmentation of nontreated cells and allicin-treated U937 cells (20 μM, 40 h, 10 μg/lane). Lane M is a DNA size marker.

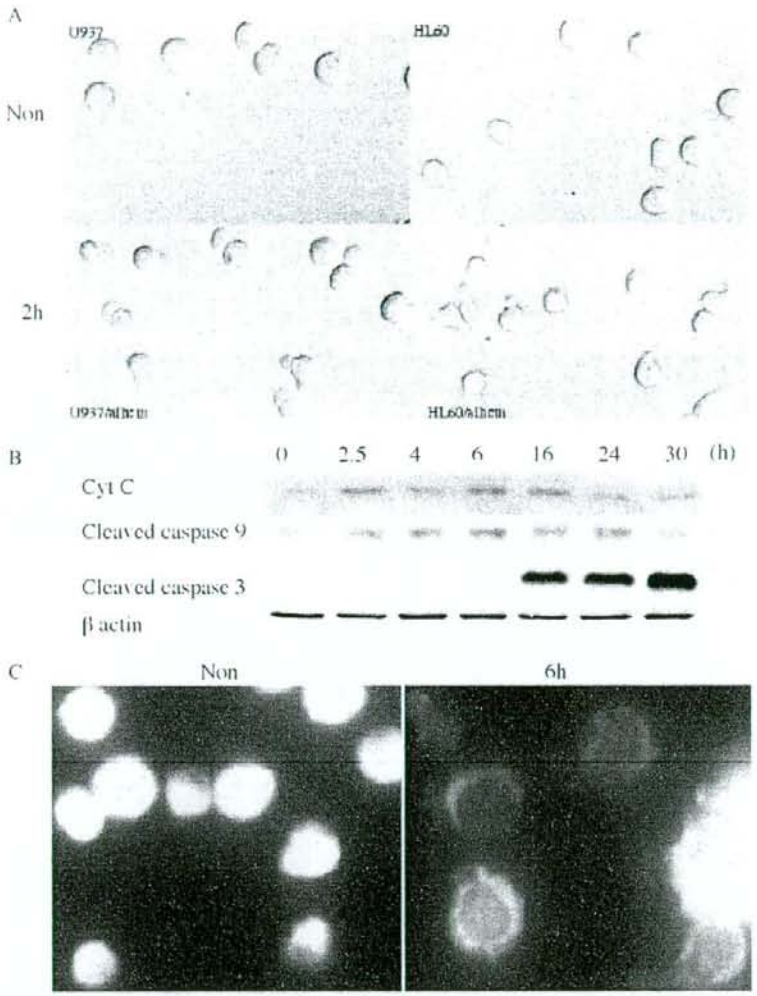

Fig. 3. (A) Morphological changes in HL60 and U937cells treated with allicin. HL60 and U937 cells treated with allicin (5 or 20 μM, respectively) for 2 h were collected and washed with PBS. Cells were visualized by confocal microscopy (original magnification ×40). (Upper panel) Nontreated cells (the diameter of 100 cells was measured). (Lower panel) Allicin-treated cells. (B) Immunoblot analysis of extracts (20 μg protein/lane) from allicin treated HL60 cells at various time of allicin (5 μM) treatment. The degrees of cytochrome *c* release into the cytosol and of caspase 9 and caspase 3 activation were assessed. β-Actin served as a control to the amount of loaded protein. The analysis of caspase 3, 9 and β-actin was done on the same blot after stripping. The data were obtained from one representative experiment (total of three independent experiments). (C) Staining of HL60 cells with MitoTracker Red CMXRos. HL60 cells treated with allicin (5 μM, 6 h) were collected, resuspended in fresh medium and were stained for 30 min with MitoTracker Red CMXRos (0.05 μM, 30 min). After washing twice with PBS, cells were examined by fluorescence microscopy (original magnification ×40).

level after 18 h. The band of cleaved caspase 9 appeared at 24 h, reached a maximal intensity at 48 h and was still seen at 72 h. Cleaved caspase 3 appeared at 30 h, became intense at 48 h and did not fade after 72 h (data not shown). Cleaved caspase 8 was not observed in either cell line after allicin treatment (data not shown).

3.2.4. Impaired mitochondrial activity

Mitochondrial activity was monitored with the XTT assay in cells treated with allicin (5 and 20 μM for HL60 and U937, respectively) for 16 h (Fig. 4). Both cell lines behaved similarly, showing a residual mitochondrial activity 65±5% in HL60 and 62±5% in U937 cells. At this stage, the drop in

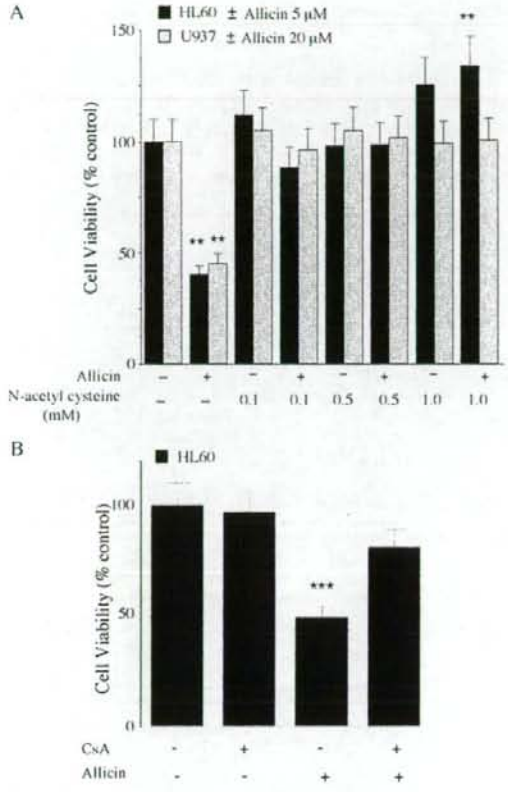

Fig. 4. (A) Allicin effect on cell viability in the absence or presence of *N*-acetyl cysteine. HL60 and U937 cells (100,000 cells/ml) were treated with allicin (5 or 20 μM, respectively) for 16 h, in the absence or presence of *N*-acetyl cysteine at 0.1, 0.5 and 1.0 mM. Cell viability was measured by the XTT assay after 3 h of incubation at 37°C with 5% CO_2. Means±S.D. of one experiment (n=6) are shown (total of three independent experiments). **P<.01 represents a significant difference from nontreated cells, based on one-way ANOVA followed by Dunnett's test. (B) Allicin effect on HL60 cell viability following a 1-h CsA (5 μM) pretreatment. HL60 cells (100,000 cells/ml) were treated with or without allicin (5 μM) for 16 h. Cell viability was measured by the XTT assay. Means±S.D. of one experiment (n=6) are shown (total of three independent experiments). ***P<.001, represents significant difference compared with nontreated cells by one-way ANOVA followed by Bonferroni's multiple comparison test.

mitochondrial activity was not accompanied by a significant change in cell number. Such a change was observed only after 24 h. Nontreated HL60 cells proliferated at a higher rate than nontreated U937 cells. Although after 24 h nontreated HL60 cells exceeded nontreated U937 cells in number, mitochondrial activity (measured by XTT assay) in U937 cells (0.869±0.025 optical density [OD] units at 450 nm, n=6) was significantly higher than that in HL60 cells (0.498± 0.073 OD units, n=6) (P<.001). These results indicate a higher battery of mitochondrial enzymes in U937 cells and suggest a higher resistance to allicin. When cells were treated with allicin in the presence of NAC (0.1–1.0 mM), mitochondrial metabolic activity was not impaired, and the antiproliferative effect of allicin was precluded (Fig. 4A).

3.3. Allicin induces changes in mitochondrial membrane potential

Nontreated cells showed strong staining with MitoTracker Red CMXRos, indicating the negative membrane potential of the mitochondria and the accumulation of the lipophilic dye. In HL60 cells treated with allicin (5 μM, 6 h the staining intensity decreased significantly, indicating changes in the mitochondrial membrane potential (Fig. 3C). Reduced mitochondrial staining in allicin-treated (20 μM) U937 cells occurred much slower; changes were observed 24 h after treatment, and the decline continued up to 40 h (data not shown).

A deeper insight into the involvement of mitochondrial permeability transition pore (mPTP) in the cytotoxicity of allicin was gained by using cyclosporine A (CsA), an inhibitor of adeninenucleotide translocator. HL60 cells were preincubated with 5 μM CsA forl h and then treated with allicin for 16 or 20 h. CsA inhibited the detrimental effects of allicin on cell viability as determined by the XTT assay (~80% residual viability for CsA pretreatment; ~50% for allicin alone). There was no significant difference between nontreated and CsA-treated cells (P>.05). No significant difference was found between CsA alone and CsA followed by allicin treated cells (P>.05) (Fig. 4B). CsA-pretreated cells were stained with Hoechst 33342 and MitoTracker Red CMXRos. CsA pretreatment prevented the nuclear condensation induced by treatment with allicin alone (Fig. 5). Mitochondrial staining also showed the preventive effect of CsA, whereby allicin-induced mitochondrial membrane depolarization was inhibited.

Fluorescence-activated cell sorting (FACS) analysis of HL60 cells treated with allicin (5 μM, 20 h) showed that 35.0% of the cells were apoptotic, whereas CsA pretreatment reduced the apoptotic fraction to 17.1% (P<.05). Cell arrest at G2 was increased in allicin-treated cells with or without CsA pretreatment 34.9% and 59.0%, respectively (Fig. 6). The fraction of HL60 cells at the G2 stage was 17.3% for nontreated cells and 18.9% for cells treated with CsA only (the difference is not significant).

3.4. Differences in GSH levels between HL60 and U937

GSH concentrations (nmol/total cell volume) in nontreated HL60 and U937 cells were almost the same: 3.4±0.48 mM and 3.7±0.55 mM, respectively. However, due to the differences in cell size between the two cell lines, analysis of GSH concentration expressed as a function of protein levels or cell numbers was also used. This analysis revealed significant differences between the GSH concentrations in the two cell lines. In nontreated HL60 cells, GSH concentration was 20.94±3.15 nmol/mg protein, and in nontreated U937 cells, 30.80±6.04 nmol/mg protein (P<.02). The

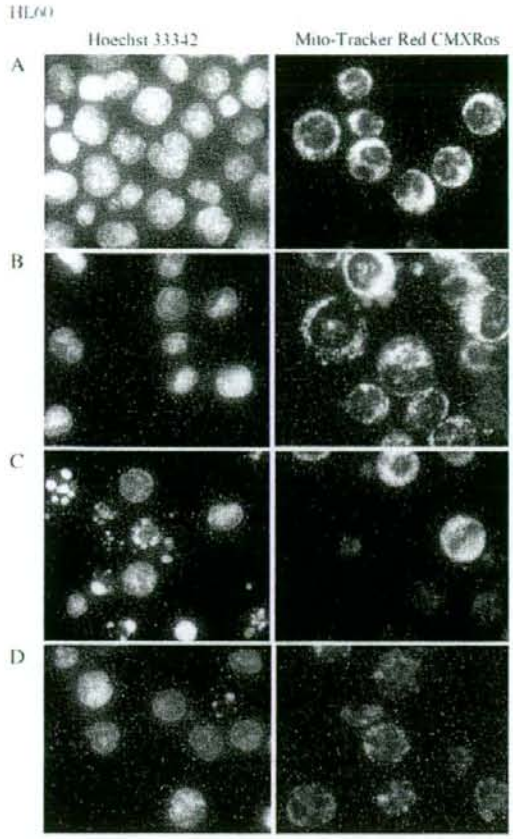

Fig. 5. Morphological effects of allicin on CsA pretreated HL60 cells. Cells (200,000 cells/ml) with or without CsA pretreatment (5 μM, 1h) were diluted and incubated in the presence or absence of allicin (5 μM) for 16 h. Cells were stained with Hoechst 33342 (5 μg/ml) or with Mito-Tracker Red CMXRos (50 nM) for 30 min. Cells were washed twice with PBS and examined by fluorescence microscopy. (A) HL60 nontreated. (B) CsA-treated. (C) Allicin-treated. (D) CsA- and allicin-treated.

difference was found to be even higher when cell numbers were considered, GSH concentration in HL60 cells was 3.7±0.56 nmol/10^6 cells whereas, in U937 cells, approximately twice as much [7.7±1.08 nmol/10^6 cells (P<.001)].

3.5. Allicin-induced GSH depletion

Allicin treatment of HL60 cells caused a rapid decrease in GSH concentration, reaching its lowest point at about 30 min. A spontaneous recovery occurred, reaching the basal level of GSH (Fig. 7A). The highest GSH levels were observed in HL60 cells between 2–24 h after adding allicin. In allicin-treated U937 cells, a decrease in GSH levels to a minimal value occurred 2–4 h after treatment, and it was followed by a gradual increase to the basal GSH level (Fig. 7B).

3.6. Allicin-induced GSH depletion in the cells pretreated with BSO

In HL60 cells treated with BSO, an inhibitor of γ-glutamyl-cysteine synthetase (GGCS) (0.4 mM, 20 h) GSH levels decreased to 1.45±0.25 nmol/10^6 cells. No cell death was observed, but there was a slight decrease in the proliferation rate (×1.7 after 20 h as compared to ×2.1 in

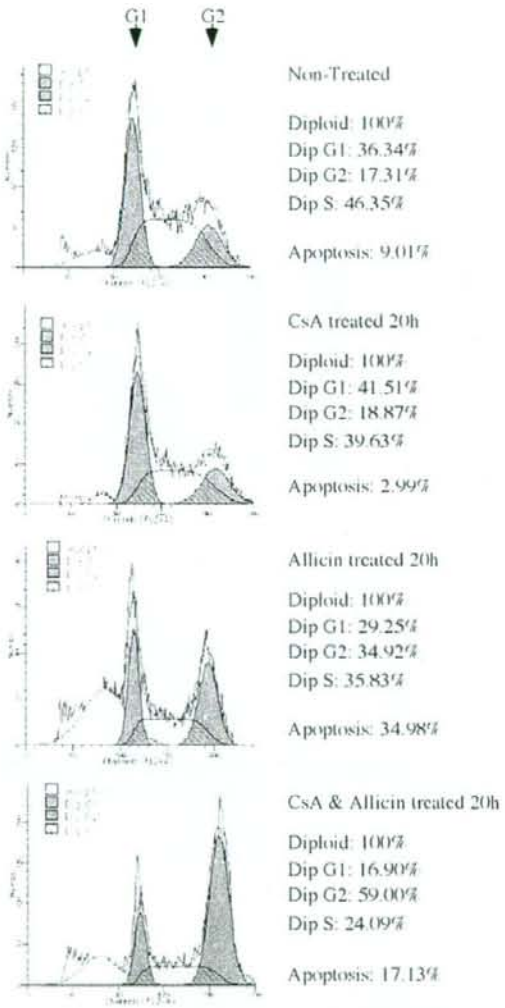

Fig. 6. Cell cycle analysis of allicin-treated HL60 cells. Cells (200,000 cells/ml, 1.5×10^6) with or without CsA pretreatment (5 μM, 1 h) were diluted and incubated in absence or presence of allicin (5 μM) for 20 h. The cells were stained with propidium iodide in the presence of RNase A and Triton X-100, as described in Materials and methods. The data represent one experiment (total of three independent experiments).

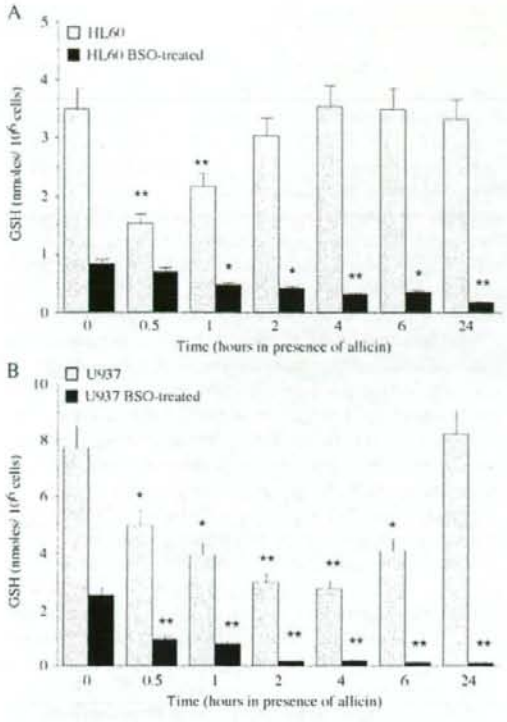

Fig. 7. Time-dependent decrease of GSH levels in allicin-treated HL60 and U937 cells after BSO pretreatment. Cells were pretreated with or without 0.4 mM BSO for 20h. HL60 and U937 cell cultures were diluted to 100,000 cells/ml and were grown in the presence of allicin (5 and 20 μM, respectively). At each time point, 30-ml samples were harvested and washed twice with PBS. Cell pellets were extracted with 5% metaphosphoric acid and analyzed for GSH content and protein concentration. Means±S.D. of one representative experiment (total of three independent experiments).

nontreated cells). Allicin (5 μM) applied to HL60 cells pretreated with BSO (0.4 mM, 20 h) caused an additional GSH decrease to 0.65±0.13 nmol/10^6 cells after 1 h (Fig. 7A, black column). There was no recovery of GSH as in the case of HL60 cells treated with allicin alone. In U937 cells pretreated with BSO (0.4 mM, 20 h), GSH levels decreased to 1.06±0.14 nmol/10^6 cells. Also, in this case, no cell death was observed and cells were still proliferating. When BSO-pretreated U937 cells were incubated with allicin (20 μM), GSH levels further decreased to 0.33±0.08 nmol/10^6 cells within 2 h (Fig. 7B, black column). A high rate of cell death (60–80%) occurred in both cell lines 24 h after allicin was applied to the culture.

3.7. Reduction potential in allicin-treated cells

Since allicin-treated cells lost their spherical structure and their volume could not be calculated from diameter measurement, we had to use another parameter to calculate changes in the intracellular reducing state resulting from fluctuations in 2GSH/GSSG ratios. Based on the assumption that 1-mg cell pellet is equivalent to 1 μl of volume, cell pellets were weighed, and GSH molar concentration was calculated accordingly (GSH amount/cell weight). Therefore, calculated reduction potential represents only approximate values. The intracellular pH of HL60 cells is 7.0 [37], and the reported E_0 for this pH is −240 mV [27]. Using the above E_0 values, reducing potential (E_{GSH}) calculated for nontreated HL60 was −207 mV (GSH 3.42±0.18 mM, GSSG 0.15±0.023 mM) and for allicin-treated (0.5 h) −169 mV (GSH 1.4±0.17 mM, GSSG 0.46±0.082 mM). The intracellular pH of U937 cells is 7.04 [38] or 7.2 [39], and the

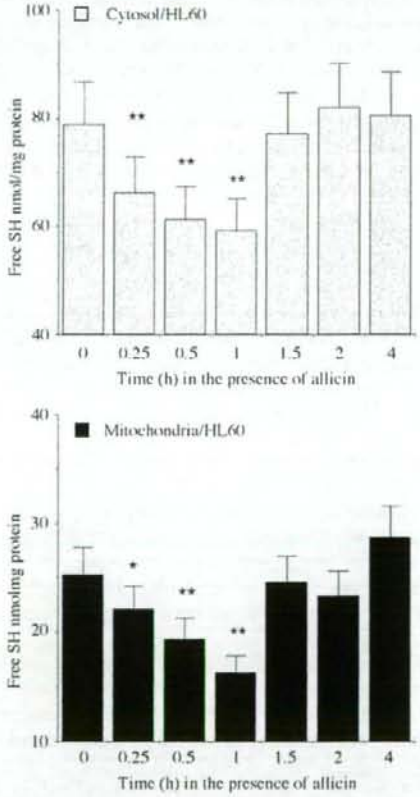

Fig. 8. Free SH contents in cytosolic and crude mitochondrial fractions from allicin-treated HL60 cells. Allicin (5 μM) was added to cells growing at density of 100,000 cells/ml. At various time intervals, 100-ml samples were harvested at 4°C, washed twice with PBS and stored at −80°C overnight. Cell fractionation was done as described in Materials and methods. Total free SH and protein concentrations were determined as described in Materials and methods. The SH content at various time intervals in the cytosol (upper panel) and in the crude mitochondrial fraction (lower panel) are shown. Means±S.D. of one representative experiment (total of three independent experiments) [40].

reported E_0 values are −240 mV or −252 mV, respectively. The calculated reducing potential values of nontreated U937 cells were −206 mV or −218 mV (GSH 3.7±0.21 mM, GSSG 0.18±0.040 mM), and for allicin-treated cells (2 h), −173 mV or −185 mV (GSH 1.54±0.042 mM, GSSG 0.41±0.021 mM). The values obtained for nontreated cells are characteristic of cells in proliferation/differentiation state, whereas those obtained after allicin treatment are typically obtained in the apoptotic state.

3.8. Free SH in the cytosolic and mitochondrial fractions of HL60 cells

Total free SH concentrations were determined in the cytosol and in the crude mitochondrial fractions prepared from allicin-treated HL60 cells. The decrease in free SH in the cytosol (Fig. 8, upper panel) was accompanied by a decrease of free SH in the mitochondria (Fig. 8, lower panel). Since mitochondrial GSH is supplied from the cytoplasm and upon allicin treatment it was depleted in both cellular compartments, it was followed by a substantial decrease in the cell-reducing potential. Consequently, depolarization of the mitochondrial membrane occurred and triggered a chain of apoptotic events leading to cell death.

4. Discussion

GSH, cysteine and accessible free SH groups of various proteins and peptides are rapidly oxidized by allicin to their respective allyl-SS derivatives [19,22]. The mixed disulfide formed is less active than allicin, yet it can easily react with free SH in thiol-disulfide exchange reactions, and produce, at the end of a series of reactions, the oxidized form of glutathione (GSSG), the oxidized form of cysteine (cystine) and glutathiolated S proteins. The leaving group (allyl-mercaptan) is volatile and rapidly disappears.

Glutathione is the major regulator of the thiol-disulfide redox state of living cells (reviewed in Refs. [29,41–43]). Alterations in cellular free thiols have already been described as a key event in the generation of apoptosis (reviewed in [44,45]).

In this study, allicin induced mitochondrial release of cytochrome *c*, activation of caspase 9 and 3 and DNA fragmentation in HL60 and U937 cell lines in a concentration- and time-dependent manner. GSH depletion had been shown to be associated with cell surface blebbing in hepatocytes [46]. Here, cell blebbing occurred in both HL60 and U937 cells treated with allicin. The rate of free SH depletion from the cytosol and the mitochondria was similar, indicating that allicin penetrated the mitochondria and the cell membrane equally well and reacted with free SH in both compartments. Allicin induced an initial drop in GSH levels that was followed by a regeneration process, occurring several hours after treatment. This may be due to decreased feedback inhibition of GSH biosynthetic enzymes such as GGCS by GSH [45]. Conversely, in BSO-pretreated cells, there was no recovery of GSH after its allicin-induced depletion, as BSO is a direct inhibitor of GGCS. BSO pretreatment in allicin-treated U937 cells shortened the life span from 72 to 20 h, indicating that preliminary GSH depletion renders cells more sensitive to apoptosis. BSO-depleted GSH levels in U937 cells were, at this stage, similar to the inherent GSH level in HL60 cells and, hence, a similar degree of sensitivity to allicin.

Here, we have shown that allicin causes GSH depletion concomitantly in the cytosol and the mitochondria in HL60 cells. It is known that active GSH uptake by intact mitochondria occurs even at very low cytosolic GSH levels and that the rate of mitochondrial GSH depletion is much slower than that of the cytosol [47]. These are indications that mitochondria have more than one control mechanism to maintain GSH levels. Since BSO-induced depletion of GSH levels caused neither mitochondrial permeability transition nor apoptosis, it is likely that BSO treatment depletes GSH mainly from the cytosol, whereas allicin induced depletion of mitochondrial GSH trigger the apoptotic process. Moreover, CsA (mPTP inhibitor) pretreatment of HL60 cells inhibits allicin-induced mitochondrial permeability transition and cell death, corroborating the central role of mitochondria in the apoptotic process induced by allicin. Simultaneous addition of NAC and allicin to cells provided protection against the apoptotic damage. NAC sequestered the harmful activity by competing with GSH for the reaction with allicin.

The following allicin-induced apoptotic scenario can be deduced from this study: Allicin penetrates the cells and readily reacts with any exposed SH present in its vicinity. As GSH is the most abundant thiol molecule in the cytosol and the mitochondria, it is the main target for allicin reaction. The reaction with glutathione leads to an immediate change in the ratio GSH/GSSG. The increased concentration of GSSG and the depletion of GSH brings about a decrease in the cellular reduction potential state. Concomitantly, mitochondrial damage occurs, as is evident from changes in membrane potential, its decreased enzymatic activity and the release of cytochrome *c* to the cytosol. Upon its release, cytochrome *c* participates in the activation of the caspase 9, followed by activation of caspase 3.

Allicin induced cell cycle arrest at G2/M in HL60 cells (~35%). Upon CsA pretreatment, the percentage of cells at G2/M was even higher (~59%). After pretreatment of HL60 cells with CsA and 40-h incubation with allicin, there was no change in the number of viable cells, neither were there signs of cell breakage. By using CsA, it could be shown that the effect of allicin on cell cycle arrest was independent of its proapoptotic activity. The mechanism by which allicin induces G2/M cell arrest is not clear, but a clue may reside in its ability to inhibit microtubule assembly. It had been shown that microtubule assembly is disrupted by direct modification of tubulin SH groups [48–50] and that adding GSH to an in vitro microtubule assembly system disrupted by SH modification restores tubulin polymerization [51].

Here we have shown that, in allicin-treated cells, there is an increase in GSH synthesis. Therefore, cell cycle arrest would be expected to expire after tubulin recovery. However, the protracted G2/M phase induced by cyclosporine A and allicin suggests an additional modification of a critical pathway that needs an extended period to regenerate.

Allicin disappears from the medium very rapidly due to its penetration into the cells and its reaction with SH group. When applied to HL60 cells (5 μM/10^5 cells/ml) or to U937 cells (20 μM/10^5 cells/ml), it could not be detected in the medium after 2 h or 6–8 h in HL60 or U937 cells, respectively. The consumption of allicin within such a short time enables full activity of SH-dependent apoptotic enzymes such as the cysteine proteases and caspases 9 and 3 [52].

Cell sensitivity to allicin was shown to be dependent on the intracellular content of GSH. Since there is a significant difference in cell size between the two cell lines examined, comparing GSH amount/cell number showed that HL60 cells contained 3.7 nmol GSH/10^6 cells, whereas U937 cells contained 7.7 nmol GSH/10^6 cells. The differences in GSH intracellular content reflect differences in sensitivity to allicin. The higher the GSH, the less sensitive to allicin cells are, and the slower the apoptotic signs appear.

The allicin-induced decrease in GSH levels modulates the redox state of cells. In allicin-treated HL60 cells, the ratio of [GSH]/[GSSG or GSSA] changed within the first 30 min and the reducing potential reached −170 mV, whereas in U937 cells, it took 2 h to reach the same level. Such a high value is typical of the apoptotic state [27].

Since GSSA (the first main product of allicin reaction with GSH) is able to prevent the formation of free radicals [19], it is likely that the initial event inducing apoptosis does not occur via the generation of reactive oxygen species but rather through mitochondrial membrane depolarization or through a more finely tuned event mediated by protein modification upon creating a mixed disulfide [19,53]. Oxidative stress incurred by the accumulation of peroxides is a secondary event probably happening after the short-lived GSSA is eliminated from the cells.

It was reported that, in BSO-treated U937 cells, the depletion of GSH and the release of cytochrome *c* into the cytosol were counteracted by cell-repair systems involving nuclear factor κB and heat shock proteins [54]. Our results show that CsA and NAC prevented apoptosis induced by allicin. Taken together, the role allicin plays may be through direct modification of specific free SH in proteins, such as reside in apoptotic repair system, in the mPTP [55] or others.

Acknowledgment

We would like to thank Dr. A. Gross, Department of Biological Regulation, Weizmann Institute of Science for critical reading of the manuscript, and Mrs. Anna Gakamsky for her help in the statistical analysis.

References

[1] Stoll A, Seebeck E. Chemical investigation on alliin, the specific principle of garlic. Adv Enzymol 1951;11:377–400.
[2] Koch HP, Lawson LD. Garlic: the Science and therapeutic application of *Allium sativum* L. and related species. 2nd ed. Baltimore: Williams & Wilkins; 1996.
[3] Elkayam A, Mirelman D, Peleg E, Wilchek M, Miron T, Rabinkov A, et al. The effects of allicin and enalapril in fructose-induced hyperinsulinemic hyperlipidemic hypertensive rats. Am J Hypertens 2001;14:377–81.
[4] Eilat S, Oestraicher Y, Rabinkov A, Ohad D, Mirelman D, Battler A, et al. Alteration of lipid profile in hyperlipidemic rabbits by allicin, an active constituent of garlic. Coron Artery Dis 1995;6:985–90.
[5] Abramovitz D, Gavri S, Harats D, Levkovitz H, Mirelman D, Miron T, et al. Allicin-induced decrease in formation of fatty streaks (atherosclerosis) in mice fed a cholesterol-rich diet. Coron Artery Dis 1999; 10:515–9.
[6] Gonen A, Harats D, Rabinkov A, Miron T, Mirelman D, Wilchek M, et al. The antiatherogenic effect of allicin: possible mode of action. Pathobiology 2005;72:325–34.
[7] Lang A, Lahav M, Sakhnini E, Barshack I, Fidder HH, Avidan B, et al. Allicin inhibits spontaneous and TNF-alpha induced secretion of proinflammatory cytokines and chemokines from intestinal epithelial cells. Clin Nutr 2004;23:1199–208.
[8] Agarwal KC. Therapeutic actions of garlic constituents. Med Res Rev 1996;16:111–24.
[9] Hirsch K, Danilenko M, Giat J, Miron T, Rabinkov A, Wilchek M, et al. Effect of purified allicin, the major ingredient of freshly crushed garlic, on cancer cell proliferation. Nutr Cancer 2000;38:245–54.
[10] Knowles LM, Milner JA. Possible mechanism by which allyl sulfides suppress neoplastic cell proliferation. J Nutr 2001;131:1061S–6S.
[11] Sun L, Wang X. Effects of allicin on both telomerase activity and apoptosis in gastric cancer SGC-7901 cells. World J Gastroenterol 2003;9:1930–4.
[12] Oommen S, Anto RJ, Srinivas G, Karunagaran D. Allicin (from garlic) induces caspase-mediated apoptosis in cancer cells. Eur J Pharmacol 2004;485:97–103.
[13] Park SY, Cho SJ, Kwon HC, Lee KR, Rhee DK, Pyo S. Caspase-independent cell death by allicin in human epithelial carcinoma cells: involvement of PKA. Cancer Lett 2005;224:123–32.
[14] Antlsperger DSM, Dirsch VM, Ferreira D, Su JL, Kuo ML, Vollmar AM. Ajoene-induced cell death in human promyeloleukemic cells does not require JNK but is amplified by the inhibition of ERK. Oncogene 2003;22:582–9.
[15] Jin Z, El-Deiry WS. Overview of cell death signaling pathways. Cancer Biol Ther 2005;4:139–63.
[16] Hsu YT, Wolter KG, Youle RJ. Cytosol-to-membrane redistribution of Bax and Bcl-X1 during apoptosis. Proc Natl Acad Sci U S A 1997;94:3668–72.
[17] Wolter KG, Hsu YT, Smith A, Nechushtan A, Xi X, Youle RJ. Movement of Bax from the cytosol to mitochondria during apoptosis. J Cell Biol 1997;139:1281–92.
[18] Miron T, Rabinkov A, Mirelman D, Wilchek M, Weiner L. The mode of action of allicin: its ready permeability through phospholipid membranes may contribute to its biological activity. Biochim Biophys Acta 2000;1463:20–30.
[19] Rabinkov A, Miron T, Mirelman D, Wilchek M, Glozman S, Yavin E, et al. *S*-allylmercaptoglutathione: the reaction product of allicin with glutathione possesses SH-modifying and antioxidant properties. Biochim Biophys Acta 2000;1499:144–53.
[20] Xiao H, Parkin KL. Antioxidant functions of selected allium thiosulfinates and *S*-alk(en)yl-L-cysteine sulfoxides. J Agric Food Chem 2002;50:2488–93.
[21] Okada Y, Tanaka K, Sato E, Okajima H. Kinetic and mechanistic studies of allicin as an antioxidant. Org Biomol Chem 2006;4:4113–7.
[22] Rabinkov A, Miron T, Konstantinovski L, Wilchek M, Mirelman D, Weiner L. The mode of action of allicin: trapping of radicals and

interaction with thiol containing proteins. Biochim Biophys Acta 1998;1379:233–44.
[23] Freeman F, Kodera Y. Garlic chemistry-stability of *S*-(2-propenyl) 2-propene-1-sulfinothioate (allicin) in blood, solvents, and simulated physiological fluids. J Agric Food Chem 1995;43:2332–8.
[24] Lachmann G, Lorenz D, Radeck W, Steiper M. The pharmacokinetics of the S35 labeled garlic constituents alliin, allicin and vinyldithiine. Arzneimittelforschung 1994;44:734–43.
[25] Miron T, Mironchik M, Mirelman D, Wilchek M, Rabinkov A. Inhibition of tumor growth by a novel approach: in situ allicin generation using targeted alliinase delivery. Mol Cancer Ther 2003; 2:1295–301.
[26] Arditti F, Rabinkov A, Miron T, Reisner Y, Berrebi A, Wilchek M, et al. Apoptotic killing of B-chronic lymphocytic leukemia tumor cells by allicin generated in situ using a rituximab–alliinase conjugate. Mol Cancer Ther 2005;4:325–31.
[27] Schafer FQ, Buettner GR. Redox environment of the cell as viewed through the redox state of the glutathione disulfide/glutathione couple. Free Radic Biol Med 2001;30:1191–212.
[28] Jonas CR, Ziegler TR, Gu LH, Jones DP. Extracellular thiol/disulfide redox state affects proliferation rate in a human colon carcinoma (Caco2) cell line. Free Radic Biol Med 2002;33:1499–506.
[29] Gilbert HF. Molecular and cellular aspects of thiol-disulfide exchange. Adv Enzymol Relat Areas Mol Biol 1990;63:69–172.
[30] Stoll A, Seebeck E. Allium compounds V. The synthesis of natural alliin and its three optical active isomers. Helv Chim Acta 1951;34: 481–7.
[31] Miron T, SivaRaman H, Rabinkov A, Mirelman D, Wilchek M. A method for continuous production of allicin using immobilized alliinase. Anal Biochem 2006;351:152–4.
[32] Nakagawa Y, Iinuma M, Matsuura N, Yi K, Naoi M, Nakayama T, et al. A potent apoptosis-inducing activity of a sesquiterpene lactone, arucanolide, in HL60 cells: a crucial role of apoptosis-inducing factor. J Pharmacol Sci 2005;97:242–52.
[33] Grinberg M, Schwarz M, Zaltsman Y, Eini T, Niv H, Pietrokovski S, et al. Mitochondrial carrier homolog 2 is a target of tBID in cells signaled to die by tumor necrosis factor alpha. Mol Cell Biol 2005;25: 4579–4590.
[34] Gornall A, Bardawill C, David M. Determination of serum proteins by means of the biuret reaction. J Biol Chem 1949;177:751–66.
[35] Anderson ME. Determination of glutathione and glutathione disulfide in biological samples. Methods Enzymol 1985;113:548–55.
[36] Riddles PW, Blakeley RL, Zerner B. Ellman's reagent: 5,5′-dithiobis (2-nitrobenzoic acid) — a reexamination. Anal Biochem 1979;94: 75–81.
[37] Restrepo D, Kozody DJ, Spinelli LJ, Knauf PA. pH Homeostasis in promyelocytic leukemic HL60 cells. J Gen Physiol 1988;92:489–507.
[38] Oehler R, Zellner M, Hefel B, Weingartmann G, Spittler A, Struse HM, et al. Influence of heat shock on cell volume regulation: protection from hypertonic challenge in a human monocyte cell line. FASEB J 1998;12:553–60.
[39] Nilsson C, Kagedal K, Johansson U, Ollinger K. Analysis of cytosolic and lysosomal pH in apoptotic cells by flow cytometry. Methods Cell Sci 2003;25:185–94.
[40] Amonkar SV, Reeves EL. Mosquito control with active principle of garlic, *Allium sativum*. J Econ Entomol 1970;63:1172–5.
[41] Powis G. Anticancer drugs acting against signaling pathways. Curr Opin Oncol 1995;7:554–9.
[42] Sies H. Glutathione and its role in cellular functions. Free Radic Biol Med 1999;27:16–21.
[43] Moran LK, Gutteridge JM, Quinlan GJ. Thiols in cellular redox signalling and control. Curr Med Chem 2001;8:763–72.
[44] Meister A. Glutathione metabolism. Methods Enzymol 1995;251:3–7.
[45] Lash LH. Mitochondrial glutathione transport: physiological, pathological and toxicological implications. Chem Biol Interact 2006;163: 54–67.
[46] Jewell SA, Bellomo G, Thor H, Orrenius S, Smith M. Bleb formation in hepatocytes during drug metabolism is caused by disturbances in thiol and calcium ion homeostasis. Science 1982;217:1257–9.
[47] Meister A. Mitochondrial changes associated with glutathione deficiency. Biochim Biophys Acta 1995;1271:35–42.
[48] Kuriyama R, Sakai H. Role of tubulin-SH groups in polymerization to microtubules. Functional-SH groups in tubulin for polymerization. J Biochem (Tokyo) 1974;76:651–4.
[49] Li M, Ciu JR, Ye Y, Min JM, Zhang LH, Wang K, et al. Antitumor activity of Z-ajoene, a natural compound purified from garlic: antimitotic and microtubule-interaction properties. Carcinogenesis 2002;23:573–9.
[50] Xiao D, Pinto JT, Soh JW, Deguchi A, Gundersen GG, Palazzo AF, et al. Induction of apoptosis by the garlic-derived compound *S*-allylmercaptocysteine (SAMC) is associated with microtubule depolymerization and c-Jun NH(2)-terminal kinase 1 activation. Cancer Res 2003;63:6825–37.
[51] Nishida E, Kobayashi T. Relationship between tubulin SH groups and bound guanine nucleotides. J Biochem (Tokyo) 1977;81:343–7.
[52] Thornberry NA. Caspases: key mediators of apoptosis. Chem Biol 1998;5:R97–R103.
[53] Patya M, Zahalka MA, Vanichkin A, Rabinkov A, Miron T, Mirelman D, et al. Allicin stimulates lymphocytes and elicits an antitumor effect: a possible role of p21(ras). Int Immunol 2004;16:275–81.
[54] Filomeni G, Aquilano K, Rotilio G, Ciriolo MR. Antiapoptotic response to induced GSH depletion: involvement of heat shock proteins and NF-kappaB activation. Antioxid Redox Signal 2005; 7:446–55.
[55] McStay GP, Clarke SJ, Halestrap AP. Role of critical thiol groups on the matrix surface of the adenine nucleotide translocase in the mechanism of the mitochondrial permeability transition pore. Biochem J 2002541;367:548.

Journal of Neurochemistry

JOURNAL OF NEUROCHEMISTRY | 2008 | 107 | 1697–1708 doi: 10.1111/j.1471-4159.2008.05738.x

A novel molecule 'shati' increases dopamine uptake via the induction of tumor necrosis factor-α in pheochromocytoma-12 cells

Minae Niwa,*,†,‡ Atsumi Nitta,† Xiaobo Cen,† Kiyoyuki Kitaichi,§ Norio Ozaki,* Kiyofumi Yamada† and Toshitaka Nabeshima†,‡

*Department of Psychiatry, Nagoya University Graduate School of Medicine, Nagoya, Japan

†Department of Neuropsychopharmacology and Hospital Pharmacy, Nagoya University Graduate School of Medicine, Nagoya, Japan

‡Department of Chemical Pharmacology, Graduate School of Pharmaceutical Sciences, Meijo University, Nagoya, Japan

§Department of Pharmacology, Faculty of Pharmaceutical Sciences, Nagasaki International University, Nagasaki, Japan

Abstract

The psychostimulant properties of methamphetamine (METH) are associated with an increase in extracellular dopamine (DA) levels in the brain, via facilitation of DA's release from pre-synaptic nerve terminals and inhibition of its reuptake through DA transporter. Recently, we have demonstrated that tumor necrosis factor-α (TNF-α) increases DA uptake and inhibits METH dependence. Moreover, we have clarified 'shati' identified in the nucleus accumbens of mice treated with METH is involved in METH dependence. In the present study, we investigated the effects of TNF-α on DA uptake in PC12 cells and established a PC12 cell line transfected with a vector containing shati cDNA to examine the precise mechanism behind the role of shati in DA uptake. Moreover, we examined the relationship between shati and TNF-α. TNF-α increased DA uptake via the mitogen-activated protein kinase kinase pathway and inhibited the METH-induced decrease in DA uptake in PC12 cells. Transfection of the vector containing shati cDNA into PC12 cells, induced the expression of shati and TNF-α mRNA, accelerated DA uptake, and inhibited the METH-induced decrease in DA uptake. These results suggest that the functional roles of shati in METH-regulated behavioral changes are mediated through inhibition of the METH-induced decrease in DA uptake via TNF-α.

Keywords: addiction, dopamine (DA) uptake, methamphetamine, shati, tumor necrosis factor-α (TNF-α).

J. Neurochem. (2008) **107**, 1697–1708.

The abuse of methamphetamine (METH) has significant psychiatric and medical consequences, including dependence, psychosis, overdose, and even death (Rawson *et al.* 2002). Drugs of abuse, including METH, modulate the activity of mesolimbic dopaminergic neurons, projecting from the ventral tegmental area to the nucleus accumbens

Received August 17, 2008; revised manuscript received October 6, 2008; accepted October 8, 2008.

Address correspondence and reprint requests to Toshitaka Nabeshima, PhD, Department of Chemical Pharmacology, Meijo University Graduate School of Pharmaceutical Sciences, 150 Yagotoyama, Tenpaku-ku, Nagoya 468-8503, Japan. E-mail: tnabeshi@ccmfs.meijo-u.ac.jp

Abbreviations used: AMPH, amphetamine; ANOVA, analysis of variance; AP, anteroposterior; cDNA, complementary DNA; CNS, central nervous system; CSF, cerebrospinal fluid; D1-R, dopamine D1 receptor; D2-R, dopamine D2 receptor; DA, dopamine; DAT, dopamine transporter; DV, dorsoventral; ERK1/2, extracellular signal-regulated kinase 1/2; FBS, fetal bovine serum; GABA, γ-aminobutyric acid; GBR 12909, [1-(2[bis(4-fluorophenyl-) methoxy]ethyl)-4-(3-phenylpropyl)piperazine] bimesylate hydrate; GFP, green fluorescent protein; GNAT, GCN5-related N-acetyltransferase; JNK, c-Jun N-termial kinase; MAO, monoamine oxidase; MAP, mitogen-activated protein; MEK, mitogen-activated protein kinase kinase; METH, methamphetamine; ML, mediolateral; NAc, nucleus accumbens; NF-κB, nuclear factor-κB; p38, p38 mitogen-activated protein kinase; PC12, pheochromocytoma-12; PCR, polymerase chain reaction; PD98059, 2-(2-amino-3-methyoxyphenyl)-4H-1-benzopyran-4-one; RIP, serine and threonine protein kinase receptor-interacting protein; RT-PCR, reverse transcription-polymerase chain reaction; shati-AS, shati antisense oligonucleotide; shati-SC, shati-scrambled oligonucleotide; SLC6, solute carrier 6; TH, tyrosine hydroxylase; TNFR I, tumor necrosis factor type I receptor; TNF-α, tumor necrosis factor-α; TRAF2, TNF receptor-associated factor 2; VMAT-2, vesicular monoamine transporter; VTA, ventral tegmental area.

(NAc) (Koob 1992; Wise 1996; Koob *et al.* 1998). The principal target for the action of METH is believed to be the dopamine transporter (DAT), which is a member of the solute carrier 6 (SLC6) gene family of Na^+/Cl^- coupled transporters that also includes the neurotransmitter transporters of norepinephrine, serotonin, glycine, and γ-aminobutyric acid (GABA) (Amara and Kuhar 1993; Torres *et al.* 2003; Chen *et al.* 2004). The DAT controls dopaminergic signaling by the rapid reuptake of dopamine (DA) from synaptic clefts. As a substrate, METH not only competitively inhibits DA uptake and thereby increases synaptic DA but also promotes the reverse transport of nonvesicular DA, resulting in an efflux of DA via the DAT (Sulzer *et al.* 2005; Fog *et al.* 2006). This efflux results in a dramatic increase in extracellular DA and is believed to be of major importance for the psychostimulant properties of METH (Sulzer *et al.* 2005; Fog *et al.* 2006). However, the exact neuronal circuits and molecular cascade essential for drug dependence are still poorly understood. Moreover, the molecules related to the METH-induced increase in DA efflux are unclear.

Tumor necrosis factor-α (TNF-α) plays an important role in a variety of infectious, inflammatory, and autoimmune conditions (Vassalli 1992). TNF-α also affects the CNS directly or indirectly through the stimulation of vagal afferents (Maier and Watkins 1998). Thus, this proinflammatory cytokine is emerging as a modulator of CNS function. Recently, we have demonstrated that TNF-α activates synaptosomal and vesicular DA uptake (Nakajima *et al.* 2004). Moreover, we have reported that TNF-α and its inducer diminish METH and morphine-induced behavioral sensitization and rewarding effects by promoting plasmalemmal and vesicular DA uptake as well as attenuating the METH and morphine-induced increase in overflow of DA in the NAc (Nakajima *et al.* 2004; Niwa *et al.* 2007b,d; Niwa *et al.* 2008). TNF-α modulates cellular responses through the extracellular signal-regulated kinase 1/2 (ERK1/2) and nuclear factor-κB (NF-κB) signaling pathways (van Vliet *et al.* 2005). ERK1/2 regulates the surface expression and capacity of DAT (Morón *et al.* 2003). However, the mechanisms by which TNF-α regulates the uptake of DA are poorly understood.

Recently, we have identified a novel molecule 'shati' in the NAc of mice treated with METH repeatedly using the polymerase chain reaction (PCR)-select complementary DNA (cDNA) substraction method, which is a differential and epochal cloning technique. Further, we have demonstrated that shati, which contains the sequence of GCN5-related *N*-acetyltransferase (GNAT), acetyl-CoA-binding sites, and ATP-binding sites, is involved in METH-induced hyperlocomotion, sensitization, and conditioned place preference (Niwa *et al.* 2007a). Blockage of shati expression by shati antisense oligonucleotide (shati-AS) potentiates not only the increase in extracellular DA levels, but also the decrease in synaptosomal and vesicular DA uptake in the NAc induced by repeated METH treatment, resulting in potentiation of the METH-induced dependence (Niwa *et al.* 2007a).

Pheochromocytoma-12 (PC12) cells are useful as a model of the neuronal system and have DATs. In the present study, we investigated the effects of TNF-α on DA uptake in PC12 cells and the involvement of the mitogen-activated protein kinase kinase (MEK) pathway in the effects of TNF-α on DA uptake. Moreover, we succeeded in the transfection of a vector containing shati cDNA into PC12 cells, investigated the involvement of shati in DA uptake and the METH-induced decrease in DA uptake, and examined the relationship between shati and TNF-α by using these PC12 cells.

Materials and methods

Cell culture and transfection

PC12 cells purchased from the Riken cell bank (No. RCB0009) were cultured on poly-ornithine-coated coverslips in Dulbecco's modified Eagle's medium (Sigma-Aldrich St Louis, MO, USA) supplemented with 10% heat inactivated horse serum and 5% fetal bovine serum (Loder and Melikian 2003). We made the vector containing shati cDNA with the suggested sequence of NM_001001985 using the plasmid pcDNA-DEST53 (Invitrogen, Carlsbad, CA, USA) as an expression vector with green fluorescent protein (GFP), although N-terminal of seven amino acids of shati was missing (CDS 882-1760) in this vector. For transient expression, the cells were transfected with the plasmid expressing shati using Lipofectamine 2000 (Invitrogen).

[^{3}H] DA uptake in PC12 cells

The uptake of [^{3}H] DA in PC12 cells was performed as described before (Melikian and Buckley 1999). The cells were washed in Krebs-Ringers- 4-(2-hydroxyethyl)-1-piperazineethanesulfonic acid buffer twice before the assay. Uptake was initiated by adding 1 μM [^{3}H] DA (Perkin Elmer, Waltham, MA, USA) containing 10^{-5} M pargyline and 10^{-5} M ascorbic acid. Uptake proceeded for 10 min at 23°C and was terminated with three rapid washes in ice-cold Krebs-Ringers-4-(2-hydroxyethyl)-1-piperazineethanesulfonic acid buffer. The amount of [^{3}H] DA accumulated was determined by liquid scintillation counting (Beckman Coulter, Inc., Fullerton, CA, USA). Non-specific uptake was defined in the presence of 10 μM [1-(2[bis(4-fluorophenyl-) methoxy]ethyl)-4-(3-phenylpropyl)piperazine] bimesylate hydrate (GBR 12909). The cells were pre-treated with TNF-α (0.1, 1, and 10 ng/mL) for 40 min, and assayed for [^{3}H] DA uptake. To neutralize TNF-α in PC12 cells, the cells were pre-treated with polyclonal goat anti-TNF-α antibody (R&D Systems Ltd., Minneapolis, MN, USA; Ab; 1, 10, 50, and 100 ng/mL) or soluble TNF receptor I (R&D Systems Ltd, sRI; 0.1, 0.5, 1, and 10 ng/mL) 10 min before the treatment with TNF-α (10 ng/mL, 40 min) (Barone *et al.* 1997), and assayed for [^{3}H] DA uptake. The function of TNF-α is mediated through two distinct cell surface receptors, TNF receptor I and TNF receptor II. The majority of TNF functions are mediated primarily through TNF receptor I, whereas TNF receptor II seems to play a role in only a limited number of

TNF responses (Hsu *et al.* 1995). Moreover, it has been reported that immunoreactivity for TNF receptor I is found in cell bodies and process of dopaminergic neurons (Boka *et al.* 1994). Therefore, we have used soluble TNF receptor I for neutralization for TNF-α. To examine the involvement of the MEK pathway in the TNF-α-induced increase in DA uptake in PC12 cells, the cells were pre-treated with a selective MEK inhibitor 2-(2-amino-3-methyoxy-phenyl)-4H-1-benzopyran-4-one (Calbiochem, San Diego, CA, USA; PD98059; 1, 10, 100, and 500 μM) 10 min before their treatment with TNF-α (10 ng/mL, 40 min), and assayed for [^{3}H] DA uptake. PD98059 was dissolved in dimethyl sulfoxide to give a concentration of 50 mM, stored in aliquots at −80°C, and diluted in Dulbecco's modified Eagle's medium to 1–500 μM immediately prior to use. To examine the effects of TNF-α on the METH-induced decrease in DA uptake in PC12 cells, the cells were pre-treated with TNF-α (10 ng/mL) 10 min before being treated with METH (1 μM, 30 min), and assayed for [^{3}H] DA uptake, following previous observations (Nakajima *et al.* 2004). Cen *et al.* (2008) have reported that METH (1 μM) decreases plasmmalemmal DAT expression in time-dependent manner (0, 5, 15, 30, 60 min), which is paralleled with the decrease in [^{3}H] DA uptake. Since treatment of METH (1 μM) for 30 min significantly decreases DA uptake compared with control group (Cen *et al.*, 2008), we have selected this time point for treatment of METH before the uptake assay. To examine the involvement of TNF-α in the shati-induced increase in [^{3}H] DA uptake in the shati-over-expressing PC12 cells, the cells were pre-treated with polyclonal goat anti-TNF-α antibody (R&D Systems Ltd, Ab; 50 ng/mL) or soluble TNF receptor I (R&D Systems Ltd, sR I; 1 ng/mL) 10 min before their treatment with METH (1 μM, 30 min), and assayed for [^{3}H] DA uptake.

Immunocytochemistry

Two antibodies against the peptide of the hypothetical protein, CNTAFRGLRQHPRTQLL (S-3) and CMSVDSRFRGKGIAKALG (S-4) unique to shati were generated. These peptides were conjugated to keyhole limpet hemocyanin and injected into rabbits six times at 1-week intervals. Serum was taken from the rabbits 1 week after the final injection. The serum was diluted 200 times for immunostaining (Niwa *et al.* 2007a).

Transfected PC12 cells attached to glass coverslips were fixed with 4% paraformaldehyde in phosphate-buffered saline for 20 min, and then blocked in 3% normal sera and 0.1% Triton X-100 for 1 h. The coverslips were incubated with primary antibodies at 4°C overnight, washed with phosphate-buffered saline, and then incubated with appropriate secondary antibodies for 2 h. Polyclonal rabbit anti-S-3 or anti-S-4 antibody (1 : 200), monoclonal mouse anti-tyrosine hydroxylase (TH) antibody (1 : 200, Chemicon, Temecula, CA, USA), monoclonal mouse anti-GFP antibody (1 : 500, Chemicon), polyclonal goat anti-rat TNF-α antibody (1 : 100, R&D Systems Ltd), and polyclonal rabbit anti-GFP antibody (1 : 100, Chemicon) served as primary antibodies. Goat anti-mouse Alexa Fluor 546 (1 : 1000, Invitrogen), donkey anti-goat Alexa Fluor 546 (1 : 1000, Invitrogen), rabbit anti-mouse Alexa Fluor 488 (1 : 1000, Invitrogen), and donkey anti-rabbit Alexa Fluor 488 (1 : 1000, Invitrogen) were used as secondary antibodies. After being washed and mounted, stained cells were observed under a fluorescence microscope (Axioskoop 2 plus). Because similar results were obtained using the anti S-3 and anti-S-4 antibodies in the immunohistochemical experiments, only the data obtained with the anti-S-4 antibody is described.

Real time reverse transcription-polymerase chain reaction

Total RNA was isolated using an RNeasy Kit (Qiagen, Hilden, Germany) and converted into cDNA using a SuperScript™ First-Strand System for RT-PCR Kit (Invitrogen). The levels of shati and TNF-α mRNA were determined by real-time RT-PCR using a TaqMan probe. The 18S ribosomal RNA was used as the internal control (Applied Biosystems, CA, USA). The shati primers used for real-time RT-PCR were as follows: 5′-TGTAAACACCCCTAA AGTGCCCT-3′ (forward; bp 2967–2989) and 5′-TCAATCCTGC ATACAAGGAATCAA-3′ (reverse; bp 3022–3045), and the Taq-Man probe was 5′-CACAGTCTGTGAGGCTCAGGTTGCCC-3′ (probe; bp 2995–3020). The amplification consisted of an initial step (95°C for 5 min) and then 40 cycles of denaturation for 30 sec at 95°C, annealing for 40 s at 59°C, and the extension time for 1 min at 72°C in an iCycle iQ Detection System (Bio-Rad Laboratories, Inc., CA, USA) (Niwa *et al.* 2007a). The expression levels were calculated as described previously (Wada *et al.* 2000).

Animals

The male C57BL/6J- wild-type mice were obtained from Slc Japan (Hamamatsu, Japan). Animals were housed in plastic cages and kept in a temperature-, humidity-, and light-controlled room (23 ± 1°C; 50 ± 5% humidity; 12 : 12 h light/dark cycle starting at 8:00 AM) and had free access to food and water, except during behavioral experiments. All animal care and use was in accordance with the National Institutes of Health Guide for the Care and Use of Laboratory Animals and approved by the Institutional Animal Care and Use Committee of Nagoya University School of Medicine. Animals were treated according to the Guidelines of Experimental Animal Care issued from the Japanese Pharmaceutical Society.

Shati-antisense oligonucleotide (shati-AS) treatment

Mice were anesthetized with pentobarbital (40 mg/kg, i.p.) and placed in a stereotaxic apparatus. The infusion cannula was connected to a miniosmotic pump (total capacity was 90 μL, Alzet 1002; Alza, Palo Alto, CA, USA) filled with shati-antisense oligonucleotide (shati-AS) or -scrambled oligonucleotide (shati-SC). The pump was implanted into the right ventricle [anteroposterior (AP) −0.5 mm, mediolateral +1.0 mm from the bregma, and dorsoventral −2.0 mm from the skull, according to the atlas of Franklin and Paxinos (1997)]. Phosphorothionate oligonucleotides were custom-synthesized at Nisshinbo Biotechnology (Tokyo, Japan) and dissolved in artificial CSF (147 mM NaCl, 3 mM KCl, 1.2 mM $CaCl_2$, and 1.0 mM $MgCl_2$, pH 7.2). The oligonucleotides were phosphorothioated at the first three bases of both the 5′- and 3′-ends, which results in increased stability and less toxicity. The sequences of shati-AS and -SC were 5′-TCTTCGTCTCGCAGAC CATGTCG-3′ and 5′-GGTCTGCTACACTGCTGCTAGTC-3′, respectively. Shati-AS and -SC were continuously infused into the cerebral ventricle at a dose of 1.8 nmol/6 μL/day (flow rate, 0.25 μL/h). Additionally, shati-SC was used as a control. Three days after the start of oligonucleotide infusion, mice were

administered METH (1 mg/kg, s.c.) for 5 days and decapitated 2 h after the final treatment (Niwa *et al.* 2007a).

Statistical analysis

All data were expressed as means ± SE. Statistical differences between two groups were determined with Student's *t*-test. Statistical differences among three groups or more were determined using a one-way analysis of variance (ANOVA), two-way ANOVA, or three-way ANOVA, followed by the Bonferroni multiple comparison test. $p < 0.05$ was regarded as statistically significant.

Nucleotide sequences

The DNA Data Bank of Japan/GenBank/European Molecular Biology Laboratory accession number for the primary nucleotide sequence of shati is DQ174094.

Results

Effect of TNF-α on DA uptake in PC12 cells

First, we investigated the effects of TNF on DA uptake in PC12 cells, since we have recently demonstrated that TNF-α activates synaptosomal and vesicular DA uptake in mice (Nakajima *et al.* 2004).

TNF-α (10 ng/mL, 40 min) increased [^{3}H] DA uptake compared with the control group ($F_{3,28} = 4.933$, $p < 0.01$, one-way ANOVA) (Fig. 1a). Moreover, we investigated whether the TNF-α-induced increase was antagonized by the anti-TNF-α antibody and soluble TNF receptor in PC12 cells. Pre-treatment with the antibody (10, 50, and 100 ng/

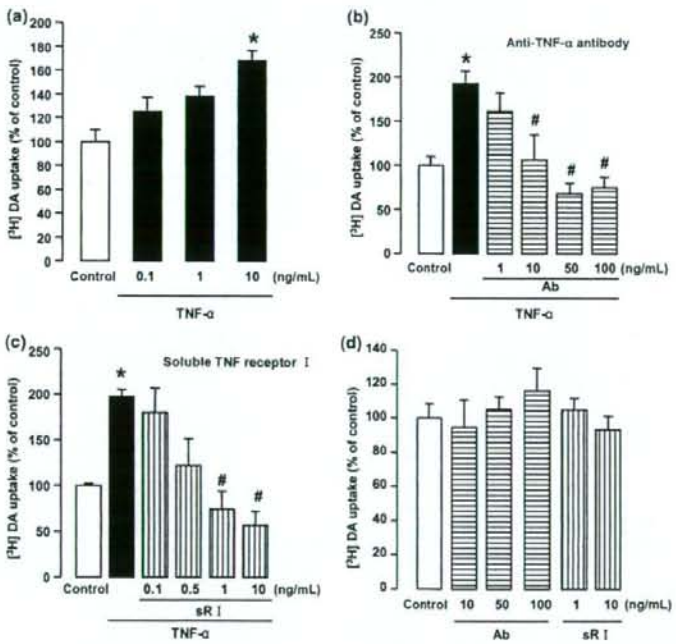

Fig. 1 Effects of anti-TNF-α antibody (Ab) or soluble TNF receptor I (sR I) on TNF-α-induced increase in [^{3}H] DA uptake in PC12 cells. (a) The cells were pre-treated with TNF-α (0.1, 1, and 10 ng/mL) for 40 min, and assayed for [^{3}H] DA uptake. The [^{3}H] DA uptake was 0.14 ± 0.01 pmol/10 min for control. The final concentration of [^{3}H] DA was 20 nM. Value are means ± SE ($n = 8$). *$p < 0.05$ versus control. (b) Effects of anti-TNF-α antibody (Ab) on TNF-α-induced increase in [^{3}H] DA uptake in PC12 cells. The cells were pre-treated with anti-TNF-α antibody (1, 10, 50, and 100 ng/mL) 10 min before their treatment with TNF-α (10 ng/mL, 40 min), and assayed for [^{3}H] DA uptake. The [^{3}H] DA uptake was 0.10 ± 0.02 pmol/10 min for the control. The final concentration of [^{3}H] DA was 20 nM. Values are means ± SE ($n = 6$–7). *$p < 0.05$ versus control. #$p < 0.05$ versus TNF-α-treated cells. (c) Effects of soluble TNF receptor I (sR I) on TNF-α-induced increase in [^{3}H] DA uptake in PC12 cells. The cells were pre-treated with soluble TNF receptor I (0.1, 0.5, 1, and 10 ng/mL) 10 min before being treated with TNF-α (10 ng/mL, 40 min), and assayed for [^{3}H] DA uptake. The [^{3}H] DA uptake was 0.06 ± 0.00 pmol/10 min for the control. The final concentration of [^{3}H] DA was 20 nM. Values are means ± SE ($n = 6$–7). *$p < 0.05$ versus control. #$p < 0.05$ versus TNF-α-treated cells. (d) Effects of anti-TNF-α antibody (Ab) or soluble TNF receptor I (sR I) on [^{3}H] DA uptake in PC12 cells. The cells were pre-treated with anti-TNF-α antibody (10, 50, and 100 ng/mL) or soluble TNF receptor I (1 and 10 ng/mL) for 50 min, and assayed for [^{3}H] DA uptake. The [^{3}H] DA uptake was 0.08 ± 0.01 pmol/10 min for the control. The final concentration of [^{3}H] DA was 20 nM. Values are means ± SE ($n = 6$–8).

mL, 50 min) or soluble TNF receptor I (1 and 10 ng/mL, 50 min) significantly inhibited the TNF-α-induced increase in [^{3}H] DA uptake ($F_{5,34} = 7.370$ for anti-TNF-α antibody; $F_{5,34} = 7.526$ for soluble TNF receptor I, $p < 0.01$, one-way ANOVA) (Fig. 1b and c), although the anti-TNF-α antibody (10, 50, and 100 ng/mL, 50 min) or soluble TNF receptor I (1 and 10 ng/mL, 50 min) itself had no effect on DA uptake (Fig. 1d). These results suggest that TNF-α activates DA uptake in PC12 cells.

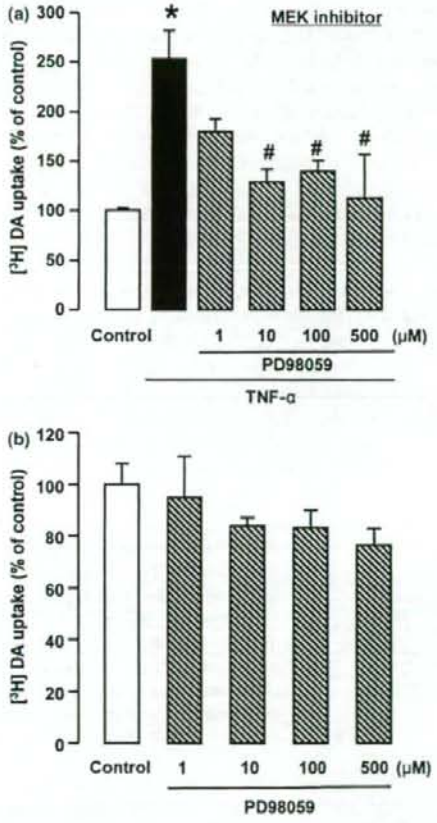

Fig. 2 Effects of MEK inhibitor on TNF-α-induced increase in [^{3}H] DA uptake in PC12 cells. (a) Effects of the MEK inhibitor PD98059 on TNF-α-induced increase in [^{3}H] DA uptake in PC12 cells. The cells were pre-treated with PD98059 (1, 10, 100, and 500 μM) 10 min before their treatment with TNF-α (10 ng/mL, 40 min), and assayed for [^{3}H] DA uptake. The [^{3}H] DA uptake was 0.10 ± 0.00 pmol/10 min for control. The final concentration of [^{3}H] DA was 20 nM. Values are means ± SE ($n = 4$). *$p < 0.05$ versus control. #$p < 0.05$ versus TNF-α-treated cells. (b) Effects of PD98059 on [^{3}H] DA uptake in PC12 cells. The cells were pre-treated with PD98059 (1, 10, 100, and 500 μM) for 50 min, and assayed for [^{3}H] DA uptake. The [^{3}H] DA uptake was 0.12 ± 0.00 pmol/10 min for the control. The final concentration of [^{3}H] DA was 20 nM. Values are means ± SE ($n = 4$).

Effects of mitogen-activated protein kinase kinase inhibitor on TNF-α-induced increase in DA uptake in PC12 cells

TNF-α modulates cellular responses through the ERK1/2 signaling pathway (van Vliet *et al.* 2005). Therefore, we investigated whether the TNF-α-induced increase in DA

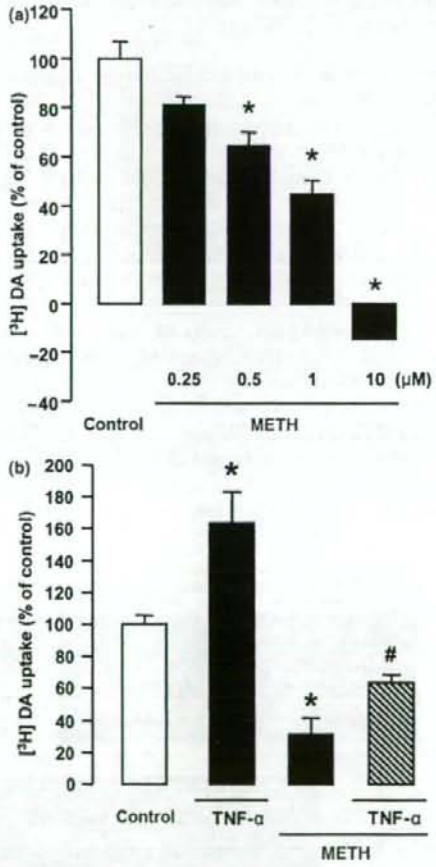

Fig. 3 Effects of TNF-α on METH-induced decrease in [^{3}H] DA uptake in PC12 cells. (a) Dose-response effects of METH on [^{3}H] DA uptake in PC12 cells. The cells were pre-treated with METH (0.25, 0.5, 1, and 10 μM) for 30 min, and assayed for [^{3}H] DA uptake. The [^{3}H] DA uptake was 0.28 ± 0.02 pmol/10 min for the control. The final concentration of [^{3}H] DA was 20 nM. Values are means ± SE ($n = 4$). *$p < 0.05$ versus control. (b) Effects of TNF-α on METH-induced decrease in [^{3}H] DA uptake in PC12 cells. The cells were pre-treated with TNF-α (10 ng/mL) 10 min before being treated with METH (1 μM, 30 min), and assayed for [^{3}H] DA uptake. The [^{3}H] DA uptake was 0.19 ± 0.01 pmol/10 min for the control. The final concentration of [^{3}H] DA was 20 nM. Values are means ± SE ($n = 5$). *$p < 0.05$ versus control. #$p < 0.05$ versus METH-treated cells.

uptake was antagonized by the MEK inhibitor PD98059 in PC12 cells.

Pre-treatment with PD98059 (10, 100, and 500 μM, 50 min) significantly inhibited the TNF-α-induced increase in [^{3}H] DA uptake ($F_{5,18} = 5.961$, $p < 0.01$, one-way ANOVA) (Fig. 2a), although PD98059 (1, 10, 100, and 500 μM, 50 min) itself had no effect on the uptake (Fig. 2b). These results suggest that TNF-α activates DA uptake via the MEK signaling pathway in PC12 cells.

Effects of TNF-α on METH-induced decrease in DA uptake in PC12 cells

We have previously demonstrated that TNF-α and its inducer diminish the METH-induced decrease in DA uptake and inhibit the rewarding effects of and sensitization to METH (Nakajima *et al.* 2004; Niwa *et al.* 2007c, e). Therefore, we confirmed the effects of TNF-α on the METH-induced decrease in DA uptake in PC12 cells.

METH (0.5, 1, and 10 μM, 30 min) decreased [^{3}H] DA uptake compared with the control group in a dose-dependent manner ($F_{4,15} = 83.675$, $p < 0.01$, one-way ANOVA) (Fig. 3a). Moreover, TNF-α (10 ng/mL, 40 min) inhibited the METH-induced decrease in [^{3}H] DA uptake (TNF-α, $F_{1,16} = 14.759$, $p < 0.01$; METH, $F_{1,16} = 45.994$, $p < 0.01$; TNF-α×METH $F_{1,16} = 1.573$, $p = 0.228$; two-way ANOVA) (Fig. 3b). These results suggest that TNF-α inhibits the METH-induced decrease in DA uptake in PC12 cells (Fig. 3) as well as promoting plasmalemmal and vesicular DA uptake to diminish METH and morphine-induced behavioral sensitization and rewarding effects (Nakajima *et al.* 2004; Niwa *et al.* 2007b; Niwa *et al.* 2008).

Transfection of the vector containing shati cDNA into PC12 cells

We established a PC12 cell line transfected with the vector containing shati cDNA to examine the role of shati in DA uptake and the METH-induced decrease in DA uptake.

We used immunostaining for TH to check morphological changes of the PC12 cells after the transfection of the vector containing shati cDNA. Morphological changes to the cells were not observed after the transfection compared with mock-transfected or non-transfected PC12 cells (Fig. 4a). To confirm the transfection of the vector containing shati cDNA, we checked for immunostaining against S-4 and GFP, co-expressed with shati. No immunoreactivity for S-4 or GFP was found in the cells that were mock-transfected, which express neither shati nor GFP [Fig. 4b (i)]. The cells mock-transfected (=expression vector [pcDNA-DEST53]), which express GFP, but not shati, were immunopositive for GFP, but not S-4 [Fig. 4b (ii)]. The cells transfected with the vector containing shati cDNA, which express both shati and GFP, were immunopositive for S-4 and GFP [Fig. 4b (iii)]. The cells immunopositive for S-4 were merged with those positive for GFP. These results indicated that shati was certainly expressed in PC12 cells and transfection did not affect cell survival or morphology.

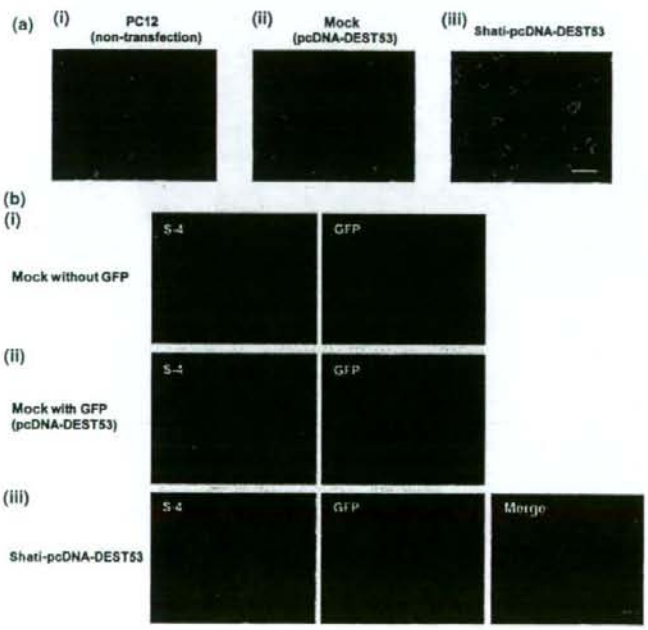

Fig. 4 Transfection of the vector containing shati cDNA into PC12 cells. (a) The morphological changes of the PC12 cells after transfection of the expression vector (pcDNA-DEST53) (ii) or vector containing shati cDNA (iii). The expression vector alone (mock-transfection) (ii), or the vector containing shati cDNA (iii) was introduced into PC12 cells. There were no changes in survival or morphology in the transfected PC12 cells. Scale bar: 20 μm. (b) Immunostaining of shati in PC12 cells transfected with the vector containing shati cDNA. pENTR/TEV/D-TOPO (without shati recombination and green fluorescent protein (GFP) site) (i), pcDNA-DEST53 with GFP (mock-transfection) (ii), or the vector containing shati cDNA and GFP (iii), was introduced into PC12 cells. The shati-immunopositive cells (green) were colocalized with GFP-immunopositive cells (red). Double immunostaining for S-4 and GFP in PC12 cells transfected with the vector containing shati cDNA reveals overexpression of shati in PC12 cells (iii). Scale bar: 20 μm.